The Astronomical Journal
Preprint typeset using LaTeX style emulateapj v. 19/02/01

INTERSTELLAR BUBBLES IN TWO YOUNG H II REGIONS

Yaël Nazé[1,2,5], You-Hua Chu[1,6], Sean D. Points[1,6], Charles W. Danforth [3,6], Margarita Rosado[4], C.-H. Rosie Chen[1]

The Astronomical Journal

ABSTRACT

Massive stars are expected to produce wind-blown bubbles in the interstellar medium; however, ring nebulae, suggesting the existence of bubbles, are rarely seen around main-sequence O stars. To search for wind-blown bubbles around main-sequence O stars, we have obtained high-resolution *Hubble Space Telescope* WFPC2 images and high-dispersion echelle spectra of two pristine H II regions, N11B and N180B, in the Large Magellanic Cloud. These H II regions are ionized by OB associations that still contain O3 stars, suggesting that the H II regions are young and have not hosted any supernova explosions. Our observations show that wind-blown bubbles in these H II regions can be detected kinematically but not morphologically because their expansion velocities are comparable to or only slightly higher than the isothermal sound velocity in the H II regions. Bubbles are detected around concentrations of massive stars, individual O stars, and even an evolved red supergiant (a fossil bubble). Comparisons between the observed bubble dynamics and model predictions show a large discrepancy (1–2 orders of magnitude) between the stellar wind luminosity derived from bubble observations and models and that derived from observations of stellar winds. The number and distribution of bubbles in N11B differ from those in N180B, which can be explained by the difference in the richness of stellar content between these two H II regions. Most of the bubbles observed in N11B and N180B show a blister-structure, indicating that the stars were formed on the surfaces of dense clouds. Numerous small dust clouds, similar to Bok globules or elephant trunks, are detected in these H II regions and at least one of them hosts on-going star formation.

Subject headings: H II regions— ISM: bubbles— ISM: kinematics and dynamics— ISM: individual (N11B, N180B) — Magellanic Clouds

1. INTRODUCTION

The fast wind of a massive star can sweep the ambient medium into a shell and form a wind-blown bubble (c.f. Weaver et al. 1977). If the ambient density is sufficiently high, the swept-up shell should appear as a "ring nebula" in Hα images. Ring nebulae are frequently seen around evolved stars with copious stellar winds, such as Wolf-Rayet (WR) stars and luminous blue variables (LBVs); however, ring nebulae are rarely seen around unevolved massive stars, such as main-sequence O stars (Chu 1991). In fact, no main-sequence O stars in the Galaxy possess well-defined optical ring nebulae.

The paucity of optical ring nebulae around unevolved massive stars is puzzling, as early-type O dwarfs may have stellar winds with terminal velocities of $\sim$2,000 km s^{-1} and mass loss rates of a few $\times 10^{-6}$ M$_\odot$ yr^{-1} (Prinja, Barlow, & Howarth 1990; de Jager et al. 1988). Three possible explanations exist: (1) no careful, systematic searches for ring nebulae around main-sequence massive stars have been conducted, (2) main-sequence massive stars preferentially reside in low density media, and (3) the microstructure of the interstellar medium prohibits the formation or the visibility of wind-blown bubbles (e.g., McKee, Van Buren, & Lazareff 1984).

To search for bubbles blown by unevolved massive stars, we have chosen to observe two young OB associations in dense H II regions in the Large Magellanic Cloud (LMC). OB associations are selected, so that a large number of stars can be imaged in the same frame. The "young age" criterion is used to avoid confusing supernova remnants (SNRs) and superbubbles, which are formed by evolved stars. The dense H II region environment is required to ensure a reasonably dense medium around the massive stars. The two OB associations we have selected are LH10 and LH117 (Lucke & Hodge 1970) in the H II regions N11B[7] and N180B (Henize 1956), respectively. Both OB associations contain O3 stars (Parker et al. 1992, hereafter PGMW; Massey et al. 1989, hereafter MGSD). The presence of O3 stars indicates that even the most massive stars have remained intact, thus suggesting a young age and enhancing the likelihood of a real absence of previous supernovae, and justifying the "pristine" state of the H II region.

[1] Astronomy Department, University of Illinois, 1002 W. Green Street, Urbana, IL 61801, USA; naze@astro.uiuc.edu, chu@astro.uiuc.edu, points@astro.uiuc.edu, c-chen@astro.uiuc.edu

[2] Institut d'Astrophysique et de Géophysique, Avenue de Cointe 5, B 4000 Liège, Belgium; naze@astro.ulg.ac.be

[3] Department of Physics and Astronomy, Johns Hopkins University, 3400 N. Charles Street, Baltimore, MD 21218; danforth@pha.jhu.edu

[4] Instituto de Astronomía IA - UNAM, Apartado 70-264, 04510 Mexico D.F., Mexico; margarit@astroscu.unam.mx

[5] Research Fellow FNRS (Belgium)

[6] Visting astronomer, Cerro Tololo Inter-American Observatory

[7] N11B is a compact H II region in the N11 H II complex. While N11 contains a known SNR, N11L, it is at 180 pc away and is totally unrelated to N11B.

The observations we have carried out for the H II regions N11B and N180B include high-resolution images obtained with the *Hubble Space Telescope* Wide Field/Planetary Camera 2 (*HST* WFPC2) and high-dispersion long-slit spectra obtained with an echelle spectrograph on the 4 m telescope at Cerro Tololo Inter-American Observatory (CTIO). Despite the high spatial resolution of the *HST* observations, few ring nebulae are found around main-sequence massive stars in LH10 and LH117.

In this paper we report the analysis of *HST* and ground-based observations of the H II regions N11B and N180B in the LMC, and use these images and spectra to investigate the issue of ring nebulae around main-sequence O stars. The observations are described in §2, the analysis and results are reported in §3, and the conclusions are discussed in §4.

2. OBSERVATIONS

The datasets used in this study include: (1) images taken with the *HST* WFPC2, and (2) high-dispersion echelle spectra taken with CTIO 4 m telescope. The high-dispersion spectra are useful to diagnose expanding shells that are not morphologically identifiable.

2.1. HST *WFPC2 Images*

HST WFPC2 images of N11B and N180B were taken on 1999 May 12 and 1998 April 29, respectively, for the Cycle 6 program 6698. For each H II region, the observations were made through the $F502N$ filter for 2×600 s and the $F656N$ filter for 2×500 s. The $F502N$ filter, centered at 5012.2 Å with a FWHM of 26.8 Å, includes only one nebular line, the [O III] λ5007 line. The $F656N$ filter, centered at 6563.7 Å with a FWHM of 21.4 Å, may include the Hα line and the neighboring [N II] lines. At the LMC's radial velocity, $\sim$300 km s^{-1}, the [N II] λ6583 line is red-shifted further away from the red edge of $F656N$'s bandpass, but the [N II] λ6548 line is red-shifted further into $F656N$'s bandpass. The filter transmission for the red-shifted [N II] λ6548 is 95% that at the red-shifted Hα. Using the [N II]/Hα intensity ratio measured from our echelle spectra (see Section 2.2), we find that the [N II] λ6548 line emission contributes to 1-2% of the $F656N$ flux of N11B, and 2-4% of that of N180B. This [N II] contamination has been corrected in our Hα flux measurements.

The calibrated WFPC2 images were produced by the standard *HST* pipeline. We process them further with IRAF and STSDAS routines. The images taken with the same filter were combined to remove cosmic rays and to produce a total-exposure map. The combined [O III] and Hα images were then corrected for the intensity- and position-dependent charge transfer efficiency by applying a linear ramp with a correction factor chosen according to the average counts of the sky background (Holtzman et al. 1995). Following the procedures for narrowband WFPC2 photometry[8], images were first divided by their total exposure time, and then multiplied by the PHOTFLAM parameter of the header, in order to get flux densities. To obtain fluxes, we multiplied the flux densities by the filter rectangular width calculated with SYNPHOT: 35.8 Å for the $F502N$ filter and 28.3 Å for the $F656N$ filter.

Figs. 1a and 1b show the large-scale environments of N11B and N180B with the WFPC2 fields marked. Figs. 1c and 1d show the WFPC2 Hα images of N11B and N180B marked with the identifications and spectral types of the most relevant stars in their OB associations (LH 10 in N11B, PGMW; LH 117 in N180B, MGSD). To better show the morphological features, we present the WFPC2 Hα images of the two nebulae individually in Figs. 2 and 3. To show the excitation variations, the [O III] images and [O III]/Hα ratio map of N11B and N180B are shown in Figs. 4 and 5, respectively.

2.2. *CTIO 4 m Echelle Spectra*

Echelle spectra were obtained with the CTIO 4 m telescope in 2000 January and December. The spectrograph was used with a 79 line mm^{-1} echelle grating and the long-focus red camera. We observed a single order centered on the Hα line by inserting a post-slit Hα interference filter and replacing the cross-dispersing grating with a flat mirror. A Tek 2048×2048 CCD with 24 μm pixel^{-1} was used to record the images. This provided a spectral sampling of 0.08 Å pixel^{-1} and a spatial sampling of $0\farcs26$ pixel^{-1}. The wavelength coverage, limited by the Hα filter and the echelle order, was 125 Å; the spatial coverage, limited by the optics, is $\sim 200''$. The angular resolution, determined by the FWHM of the seeing, was approximately $1''$. A slitwidth of $1\farcs65$ was used. The resultant spectral resolution, measured from the Th-Ar lamp lines is about 13 km s^{-1} FWHM.

The journal of observations is given in Table 1. When multiple exposures existed for a given position, they were combined taking into account their exposure times[9]. On the whole, nine slit positions were observed in N11B and four in N180B. They were all oriented either north-south or east-west; their exact positions were indicated by the arrows in Figs. 1c and 1d. The identifications of lines detected in the echelle observations are shown in Fig. 6. The spectral lines include nebular Hα and [N II] lines, and telluric OH lines (Osterbrock et al. 1996). The rest wavelengths of the nebular lines we have adopted are Hα λ6562.7885 Å, and [N II] λ6548.0800 Å and λ6583.4540 Å (Spyromilio 1995).

3. ANALYSIS AND RESULTS

For each nebula, we first describe the overall Hα morphology and surface brightness variations, and derive the rms electron density for various regions. We then identify morphological features that might have been produced by stellar winds interacting with the ambient interstellar medium, as seen in the WFPC2 Hα images. We further use the [O III]/Hα ratio map to determine whether a morphological feature has an anomalous [O III]/Hα ratio. An elevated [O III]/Hα ratio is indicative of a higher temperature or a shock excitation, while a lower [O III]/Hα ratio suggests a lower excitation or ionization. Next we describe the kinematic features detected in the echelle spectra, fit Gaussian components to the line profiles, and use the re-

[8] available at http://www.stsci.edu/instruments/wfpc2/Wfpc2_faq/wfpc2_nrw_phot_faq.html

[9] Two observations EW of PGMW 3168 were taken. Since they were not centered at the same position, we did not combine them and analyze them individually

sultant velocities to identify expanding structures and to determine expansion velocities. Finally, we combine the morphological and kinematic information and present an integrated view of the structure of the H II region.

3.1. *N11B*

3.1.1. *Surface Brightness and Density*

The H II region N11B is a young star-forming region dotted with numerous bright-rimmed dusty features. The OB association LH10 has a high concentration of stars at the southwestern part of N11B, centered near $4^h56^m44^s$, $-66°25'00''$ (see Fig. 1c). To the north of this concentration is the brightest Hα emission region mixed with dusty features and connected with several long filaments. The other members of LH10 are loosely distributed within N11B, together with small ($\sim$1 pc in size) dust clouds that are similar to Bok globules (Garnett et al. 1999) or elephant trunks (Hester et al. 1996). The two most prominent small dust clouds are situated close to luminous stars, so their surfaces are ionized and emit strongly in Hα: the kiwi-shaped dust cloud to the west of PGMW 3204 and PGMW 3209, and the Y-shaped dust cloud to the west of PGMW 3223 (see Fig. 1c). Interestingly, the tip of the Y-shaped dust cloud harbors a bright star, and our echelle observations (§3.1.3) show that this bright star has a strong Hα emission line. Several smaller dust clouds are present but at larger distances from luminous O stars, so their Hα surface brightnesses are not as high as those close to luminous O stars.

To quantitatively analyze these images, we have measured the Hα surface brightness in several regions of interest. We then compute the emission measure, EM, using: $EM = 2.41 \times 10^3\ T^{0.92}\ S(\mathrm{H}\alpha)$ pc cm^{-6}, where T is the electron temperature and $S(H\alpha)$ is the intrinsic surface brightness in units of ergs cm^{-2} s^{-1} sr^{-1} (Peimbert, Rayo, & Torres-Peimbert 1975). Adopting an electron temperature of 10^4 K and assuming that the depth of emitting material along the line of sight is similar to the observed size of a morphological feature, we may further estimate the rms electron density of the emitting material. If the feature is not spherical, the observed width (the shorter dimension) and length (the longer dimension) are used as the path-length of emission to determine the upper and lower limits of the rms density, respectively.

We assume that the density structure of N11B consists of local density enhancements superposed on a global, uniform component. For the global component, we have measured the surface brightness of a featureless region at 9″ east and 1.″4 north of PGMW 3168, and derived $S(H\alpha)$ = 9.6×10^{-4} ergs cm^{-2} s^{-1} sr^{-1}, corresponding to an EM$_{global}$ of 1.1×10^3 cm^{-6} pc, taking into account an interstellar absorption with an E(B-V) value of 0.17 (PGMW). The size of N11B, measured from the Hα image in Fig. 1a, is 257″ × 140″, or 64 pc × 35 pc for a distance of 50 kpc. The rms electron density of the global component in N11B is thus 13 to 18 cm^{-3} in N11B. We have measured the density enhancements in several arcs and the bright ionized surface of the kiwi-shaped dust cloud. The intrinsic surface brightness, excess emission measure ($EM - EM_{global}$), size of the feature, and the range of rms density of these features are listed in Table 2. It can be seen that the moderately bright arcs and filaments have rms densities of 50-150 cm^{-3}, while the bright ionized surfaces of dust clouds have rms densities several times higher.

3.1.2. *Morphology and Excitation*

Whereas there are a large number of O stars in N11B, only two of them (PGMW 3120 and PGMW 3160) are surrounded by filamentary features that are commonly identified as ring nebulae. The star PGMW 3120, classified as O5.5V((f*)) by PGMW, is surrounded in the northeast by a small arc-like structure at $\sim 5''$ from the star. The arc does not stand out in the [O III]/Hα ratio map, suggesting a similar excitation to the background H II region, or a lack of strong shock excitation. The star PGMW 3160, a K I star, is in a faint void bordered in the southwest by a bright filament $\sim 20''$ long. This filament has a lower [O III]/Hα ratio than the background H II region; however, the filament does not appear to be associated with an obvious dusty feature.

A few stars are surrounded by faint filaments, e.g., PGMW 3239 (B2V), PGMW 3157 (BC1Ia), and PGMW 3102 (O7V). Some stars, e.g., PGMW 3089 (O8V), are inside regions with suppressed surface brightness, indicating lower densities around the star, as in a cavity. None of these features stand out in the [O III]/Hα ratio map; therefore, from their excitation alone, they are indistinguishable from the background H II region, indicating that they are not shock-excited.

While no sharp, high-[O III]/Hα features are detected, many prominent low-[O III]/Hα features are present, and most of them are associated with dusty features. The correlation between low [O III]/Hα ratios and dusty features can be illustrated by the analysis of an isolated dust cloud. We use the kiwi-shaped dust cloud as an example. Figure 7 shows that the low-[O III]/Hα region delineates the surface of the dust cloud. The Hα and [O III] surface brightness profiles along a north-south cut across the kiwi-shaped dust cloud show that the Hα emission and [O III] emission on the cloud surface peak at the same location, but the [O III] emission drops off faster into the dust cloud than the Hα emission, causing a dip in the [O III]/Hα ratio. Therefore, the low [O III]/Hα ratios on the surface of a dust cloud is caused by a lower ionization and excitation. This kiwi-shaped dust cloud and the Y-shaped dust cloud are both strongly ionized on the sides facing the O3III(f*) star PGMW 3209, the earliest and most luminous O star in the vicinity. These dust clouds are most likely illuminated and ionized by this O star.

3.1.3. *Kinematic Properties*

To identify kinematic features caused by wind-ISM interactions, we examine the velocity profiles of both Hα and [N II] λ6584 lines. The [N II] line shows line splitting more easily because its thermal width is smaller than that of Hα, but the [N II] line is much weaker than the Hα line and is usually noisier. Variations of ionization condition ([N II]/Hα ratio) among different velocity components also contribute to differing appearances of the Hα and [N II] line profiles. These effects are illustrated in Fig. 8, where two pairs of Hα and [N II] line profiles are shown.

We fit Gaussian components to both Hα and [N II] profiles; the resultant velocity components plotted along each slit are presented in Fig. 9. To compare the kinematic

and morphological properties, in Fig. 10 we mark the regions with more than one velocity component along the slits, with the brighter components marked in thick solid lines and the weaker components in thick dashed lines. All quoted velocities are heliocentric. Four echellograms of the [N II] line with line-splitting are shown in Fig. 11.

A completely different view emerged when we examined the echelle spectra and used the kinematic information to identify features caused by wind-ISM interactions. The kinematic structure of N11B has been studied by Rosado et al. (1996) using imaging Fabry-Perot observations at an $18''$ resolution ($9''$ pixel^{-1}). They reported six expanding regions, designated a-f. To study these expanding regions at a higher angular resolution, we have chosen our first six slit positions centered on stars in these regions. The other slit positions were selected to study morphologically identified features: the Y-shaped dust cloud and the small ring nebula around PGMW 3120. Below we review the kinematic features along individual slits. The spectral types of the reference stars and the names of the expanding regions of Rosado et al. (1996) are noted in parentheses.

1. EW of PGMW 3204 (O6-7V; Region a):
The Hα and [N II] lines are significantly broader in the region near the O3III(f*) star PGMW 3209. The Hα and [N II] lines can be fit by two Gaussian components centered at 288 km s^{-1} and 310 km s^{-1}. The velocity plot shows a clear expanding shell structure, with an expansion velocity of $\sim$ 10 km s^{-1}. This expanding shell can be traced from $2''$ west to $54''$ east of PGMW 3204, corresponding to a linear size of 14 pc. Interestingly, the kiwi-shaped dust cloud is located right at the western edge of the expanding shell, suggesting again that this dust cloud is physically close to PGMW 3204. Despite the clear expanding shell structure revealed in the velocity plot, there are no morphological features in the WFPC2 Hα image that can be unambiguously identified as a ring nebula or an expanding shell. Outside this expanding shell, both Hα and [N II] lines can be fit well by a single Gaussian component, centered at 298 km s^{-1} on the east side and 293 km s^{-1} on the west side of the shell. The western end of the slit reaches the bright H II region north of PGMW 3120. The velocity profiles in the bright H II region are more or less Gaussian, peaking at 297 km s^{-1}, but additional faint components are detected in the region bounded by the two arcs extending from the H II region to the east.

2. EW of PGMW 3224 (O6III; Region b):
No clear line splitting is seen in the spectra along the slit, but an additional faint blue component sometimes creates a small asymmetry in the line profiles. From $63''$ east to $7''$ west of PGMW 3224, both lines display a faint blue component at 282 km s^{-1}, while the brighter component peaks at 303 km s^{-1}. Further east, the Hα line shows only one peak at 299 km s^{-1}. Further west, the line profiles peak at 299 km s^{-1} but become asymmetric again at $38''$ to $60''$ west of PGMW 3224, in the vicinity of PGMW 3160 (early KI). At the western end of this slit position, the Hα line shows an additional component at red-shifted velocities; this component is too faint to be detected in the [N II] line.

3. EW of PGMW 3168 (O7II(f); Region c):
Along this slit position, no clear line splitting is seen, but the peak velocities show a large scatter and the line profiles are often asymmetric, indicating multiple velocity components. At $133''$ to $50''$ east of PGMW 3168, both lines show Gaussian profiles centered on 298 km s^{-1}. At $50''$ to $23''$ east of the star, the Hα line is broad and shows large velocity variation, while the [N II] line profiles are noticeably asymmetric and require two velocity components in the spectral fits. The spectral fits to the [N II] line show an expanding shell with an expansion velocity of 12 km s^{-1} and a diameter of $\sim 40''$ (or 10 pc). This shell might be associated with the uncataloged star between PGMW 3223 and PGMW 3224. Near PGMW 3168 and to its west, the [N II] line also presents a main component (at 298 km s^{-1}) and a fainter blue component (at 283 km s^{-1}), although the Hα line shows Gaussian profiles centered at 295 km s^{-1}. Further west, near the bright H II region, the Hα line also show asymmetric profiles indicating velocity components at 290 and 307 km s^{-1}. Still further west (more than $67''$ west of the star), both lines seem split but the red component is quite faint. This kinematic feature does not have any morphological counterparts in the WFPC2 images.

4. NS of PGMW 3058 (O3V((f*)); Region d)[10]:
From $8''$ north of PGMW 3058 northwards, both Hα and [N II] lines exhibit clear line-splitting. It is interesting to note that a bright knot appears in the red component at $25''$ north of PGMW 3058, where the WFPC2 image shows a bright filament. (An example of such emission knot can be seen in the echelle image of PGMW 3053 slit in Fig. 11.) South of the star, the Hα line is clearly split with extreme velocities reaching 283 and 325 km s^{-1}, indicating an expansion velocity of $\sim$20 km s^{-1}. At $13''$ to $40''$ south of the star, in the vicinity of PGMW 3061 (O3III(f*)), an additional, high-velocity component at 357 km s^{-1} is detected. It is not clear whether this high-velocity feature is accelerated by the powerful stellar wind of PGMW 3061 because similar high-velocity feature is detected along the NS slit at PGMW 3120 only at a declination $20''$ south of PGMW 3061 (see description of the slit NS of PGMW 3120 below).

5. NS of PGMW 3053 (O5.5I-III(f); Region e):
This slit position is only $8''$ east of the slit along NS of PGMW 3058, thus shows a very similar kinematic structure. The line-splittings and high-velocity features detected along the slit centered on PGMW 3058 are all confirmed in the spectra along the slit centered on PGMW 3053. The bright emission knot in the red component that corresponds to

[10] Note that Rosado et al.'s (1996) Region d is centered on PGMW 3061, about $22''$ south of PGMW 3058.

a bright filament to the north of PGMW 3053 is clearly seen in Fig. 11.

6. NS of PGMW 3157 (BC1Ia; Region f):
To the north of the star, the line profiles are mostly Gaussian and centered at 297 km s^{-1}; however, at 43″ to 56″ north of the star, an additional faint blue component appears at 284 km s^{-1} and the main component becomes slightly red-shifted to 301 km s^{-1}. This region, as marked in Fig. 10, corresponds to the arc feature around PGMW 3160 (early KI). Similar velocity structure is seen in the vicinity of PGMW 3160 in the echelle slit EW of PGMW 3224. From PGMW 3157 southward to 29″ south, an additional red component is present at ∼ 310 km s^{-1}. This is the region to the south of a bright filament (see Fig. 10). Similar velocity structure in the vicinity is seen in the observation along the slit EW of PGMW 3204.

7. EW of PGMW 3223 (O8.5IV):
This slit position is selected to sample the Y-shaped dust cloud at ∼ 8″ west of PGMW 3223. The line profiles are clearly split into 287 and 306 km s^{-1} over an extent of ∼ 52″ (or 13 pc) around PGMW 3223, with the Y-shaped dust cloud situated on the western edge. The echelle spectrum of the Y-shaped dust cloud also shows an embedded star with bright Hα emission. This Hα-emission star, marked as "Hα star" in Figs. 1c and 9, is probably a newly formed massive star. Similar velocities are also recorded at 67 to 86″ west of PGMW 3223, corresponding to extensions of the bright H II region. Everywhere else, the line profiles are purely Gaussian and are centered at ∼296 km s^{-1}.

8. EW and NS of PGMW 3120 (O5.5V((f*))):
These two slit positions are selected to study the ring nebula around PGMW 3120. As seen in the WFPC2 Hα image (Figs. 1c and 2), this ring nebula is incomplete with a radius of 3″–6″. Both the Hα and [N II] lines are clearly split, with the two components at 281 and 306 km s^{-1}. However, the spatial extent of the region with line-splitting is from 12″ east to 26″ west of the star and from 7″ north to at least 40″ south of the star. This expanding shell is much more extended than the morphologically identified ring nebula, and encompasses the nearby O7V star PGMW 3102 (see Figs. 9 and 11). The small Hα arc structure is probably fortuitous. At 40″ to 54″ south of PGMW 3120, high-velocity gas at ∼347 km s^{-1} is seen. This region is within Rosado et al.'s (1996) region d, and the velocity features are similar to those within region d sampled by the NS echelle slits centered on PGMW 3058 and PGMW 3053. The eastern part of the EW slit samples part of Rosado et al.'s (1996) region a. Near stars PGMW 3204 and 3209, the Hα line is split into 287 and 308 km s^{-1}, similar to those seen in the observation along the EW slit centered on PGMW 3204.

3.1.4. *Integrated View of N11B*

The analysis of the echelle observations of N11B shows clearly that expanding shells and high-velocity, accelerated material exist in this young H II region. Most of the expanding shells do not show identifiable morphological counterparts, while the morphologically identified ring nebulae do not show expanding shell structures.

Most of the expanding shells encompass groups of massive stars; only a few surround single massive stars. Some irregular expanding features with expansion velocities 10–15 km s^{-1} are detected, but no clear association with massive stars can be identified. The expanding shells and high-velocity features associated with recognizable massive stars are described below and summarized in Table 3. The spectral types and expected wind luminosity, calculated using the wind velocities from Prinja, Barlow, & Howarth (1990) and the mass loss rates from de Jager et al. (1988), are also given in this table.

The shell encompassing the large concentration of massive stars at the SW corner of N11B corresponds to Rosado et al.'s region d. This shell has the largest expansion velocity, ∼20 km s^{-1}, and the largest dimension, ≥20 pc (see the velocity plots of NS of PGMW 3053, PGMW 3058, and PGMW 3120 in Fig. 9). The south boundary of this shell is unknown, as it is not covered in our echelle slits. The second largest shell corresponds to Rosado et al.'s region a. This shell encompasses the concentration of stars including PGMW 3204, PGMW 3209, and PGMW 3223. Its expansion velocity is ∼10 km s^{-1} and its diameter is ∼14 pc (see, e.g., the velocity plot of EW of PGMW 3204 in Fig. 9).

One expanding shell might be associated with a single star, the uncataloged bright star between PGMW 3223 and PGMW 3224. This shell has an expansion velocity of ∼12 km s^{-1}, and a diameter of ∼10 pc (see the velocity plot of PGMW 3168 in Fig. 9). A high-velocity feature, red-shifted by ∼60 km s^{-1} and extending over ∼7 pc, is detected near PGMW 3061, an O3III(f*) star (see the velocity plots of NS of PGMW 3053 and PGMW 3058 in Fig. 9). It is possible that PGMW 3061 is responsible for its acceleration. The most interesting expanding structure around a single massive star belongs to PGMW 3160, an early KI supergiant. An expanding blister structure, with a size of ∼5 pc and expansion velocity of ∼ 15 km s^{-1}, is detected in the vicinity of this red supergiant (see the velocity plot of NS of PGMW 3157). This expanding structure is most likely produced by the O star progenitor of PGMW 3160 during the main sequence stage.

Three characteristics appear to be common among the expanding shells in N11B. First, shells encompassing small numbers of massive stars have sizes of 10–15 pc and expansion velocities of 10–15 km s^{-1}, barely supersonic for an isothermal sound velocity of 10 km s^{-1} at 10^4 K. Only the shell encompassing a large number of stars is larger and expands faster. Second, Most of the expanding shells have the massive stars displaced from the shell centers, indicating a blister-like structure. Finally, some shells might be merging together and the boundaries between them become unclear.

3.2. *N180B*

3.2.1. *Surface Brightness and Density*

The most remarkable feature in the WFPC2 Hα image of N180B is the prevalence of dust clouds in different sizes and shapes. There are 30-pc-long dust streamers running across the face of the H II region, prominent antenna-shaped dust cloud at the northeastern corner of the field, large patches of dust clouds at the northwestern and southwestern corners of the field, and Bok-globule-like small dust clouds embedded in ionized gas near the large dust clouds. These dusty features amply portray a young star formation region.

The Hα surface brightness is heavily modulated by the large-scale dusty features. The brightest emission region in N180B is located in the southwestern quadrant of N180B. Its V-shaped rim is dotted with four bright O and B stars: MGSD 152, MGSD 184, MGSD 187, and MGSD 197 (see Fig. 1d for the positions and spectral types). As shown below, this higher surface brightness is caused by a higher density in this region.

Again, we have adopted a simplistic two-density-component model for the structure of N180B: a global uniform component and local density enhancements. We measured the surface brightness of a featureless region at $3\farcs5$ north and $17''$ west of the star MGSD 119 to represent the global component. Adopting a diameter of $225''$ (or 56 pc) for N180B and an E(B-V) value of 0.12 (MGSD), we derive a rms density of $\sim$9.5 cm^{-3}. We have measured the surface brightness of the bright, V-shaped emission region and the arc around MGSD 218. The rms densities of these two regions are a few $\times$10 cm^{-3}. The results are detailed in Table 2.

3.2.2. *Morphology and Excitation*

Of all stars in the WFPC2 Hα image of N180B, only two stars, MGSD 174 and MGSD 218, are surrounded by small ($5'' - 10''$) arcs or circular filaments that can be identified as ring nebulae. No spectral classification was available for these two stars, but the UBV photometric data and extinction reported by MGSD suggest that the spectral type of MGSD 174 is B2V and MGSD 218 B5V. A few stars may be associated with faint nebular features, such as a small circular emission region around MGSD 82 and the "comet-tail" of MGSD 106; however, these morphologies do not suggest a bubble structure.

The average [O III]/Hα ratio of N180B is high, $\sim$0.9, comparable to that of N11B. In the [O III]/Hα ratio map of N180B, most dust clouds, but not the long dusty streamers, are seen as regions with low [O III]/Hα ratio, $\sim$0.4. The dusty streamers across the face of the H II region show [O III]/Hα ratios similar to that of the overall H II region itself. The [O III]/Hα ratio map of N180B appears much more uniform than that of N11B. Again, no sharp, shock-excited features are identified.

The small dust cloud near MGSD 168 has [O III]/Hα ratios of 0.6–0.9, which are higher than those in N11B, such as the kiwi-shaped dust cloud. This difference is probably caused by the contamination of background/foreground emission. MGSD 168 is a mid B star, so the Hα emission from its neighboring dust cloud is weak compared to the background Hα emission from gas ionized by early O stars, while the kiwi-shaped dust cloud in N11B is ionized by early O stars and its emission is much brighter than the background emission. Therefore the low [O III]/Hα ratio in the ionization front can be more easily seen in dust clouds near early O stars than later O or B stars.

The arc around MGSD 218 has a low [O III]/Hα ratio, 0.45, indicating a low excitation at an ionization front. This kind of arc nebulae is frequently seen around early B main sequence stars near dust clouds, e.g., LSS 3027 in the Galaxy (Chu 1983). MGSD 218 is a mid B main sequence star and could be luminous enough to produce a small H II region. The filamentary nebula around MGSD 174 may also have a low [O III]/Hα ratio, but the S/N ratio of this region (imaged by the Planetary Camera of WFPC2) is too low to confirm the low [O III]/Hα ratio.

Many nebular morphological features "disappear" into the background in the [O III]/Hα ratio map. The small "comet-tail" nebulosity of MGSD 106 and the large (20 pc in size), bright, V-shaped emission region both show [O III]/Hα ratios similar to the average ratio of the entire H II region. It is interesting to note that MGSD 118 (O4 IIIf* star) is surrounded by a small emission region (size = $3''$) with a very high [O III]/Hα ratio ($\sim$1.5), but this small nebula does not show any peculiar kinematic properties (see Section 3.2.3).

3.2.3. *Kinematic Properties*

The kinematic structure of N180B is much more quiescent than that of N11B. Line splitting is seen only in the [N II] line within one expanding shell centered on MGSD 214 (O3-4). The Hα line is narrow with an observed FWHM of $\sim$30 km s^{-1}. Quadratically subtracting the instrumental FWHM of 13 km s^{-1} and a thermal FWHM of 21 km s^{-1} (assuming 10^4 K) from the observed width, we obtain a turbulent FWHM of only 17 km s^{-1}.

Figure 12 shows the velocity components of the Hα and [N II] lines along each slit. Regions with more than one velocity component are marked on the Hα image in Fig. 13. The kinematic features along each slit position are described below.

1. NS of MGSD 118 (O4IIIf*):
   The northern part of this slit, including the location of MGSD 118, show narrow Hα and [N II] lines centered at 245–250 km s^{-1}. From $28''$ south of MGSD 118 southward, the Hα line shows an additional faint blue component, which has an extreme velocity at 220–225 km s^{-1}. This suggests an expanding "blister", with the far side roughly at the H II region's systemic velocity and the near side expanding toward us with an expansion velocity of $\sim$20 km s^{-1}. The northern edge of the region appears to be bordered by a broad arc-like structure.

2. EW of MGSD 140 (O3-4(f*)):
   Along the entire slit, the Hα line appears to be a perfect Gaussian profile centered at $\sim$240 km s^{-1}, while the [N II] line shows asymmetric line profiles indicating the existence of at least two velocity components. Spectral fits of the [N II] line yield components separated by $\leq$20 km s^{-1}. The [N II] line is weak and noisy, and thus the velocity components show a large velocity scatter.

3. EW and NS of MGSD 214 (O3-4):
   From $50''$ east to $40''$ west of MGSD 214, both Hα

and [N II] lines show a bright component at 240–245 km s^{-1}, near the H II region's systemic velocity, and a faint blue component at 220–225 km s^{-1}. This velocity pattern suggests a "blister" expanding toward us. The N-S slit position shows that this expanding blister extends from ∼65″ north to ∼ 25″ south of MGSD 214. Outside this expanding blister region, the Hα and [N II] lines are both narrow. Velocity gradients are seen along both slits, from one side of the expanding blister to the other side. It is not clear whether the velocity variation of the bright component is attributed largely to the velocity gradient in the H II region or an expansion velocity variation in the receding side of the blister.

3.2.4. *Integrated View of N180B*

N180B is much more quiescent than N11B. Only one expanding blister is unambiguously detected around the O3-4 star MGSD 214. This blister is ∼22 pc in diameter and expanding away from the dense cloud at ∼20 km s^{-1} (see Table 3). No morphological counterpart of this expanding blister can be confidently identified. Two other stars have similar spectral types, MGSD 118 of type O4 IIIf* and MGSD 140 of type O3-4 (f*), but do not show unambiguous expanding shells or blisters around them. The FWHM of the Hα line in the vicinity of these two stars suggests a turbulent component of ≤17 km s^{-1} FWHM, while the [N II] line shows additional faint blue components. It is possible that these two massive stars have blisters expanding at ≤10 km s^{-1}.

The overall kinematic structure of N180B exhibits two characteristics. First, the H II region itself has a velocity gradient or variation at a level of ∼10 km s^{-1} across the nebula. Second, the expanding shells have a "blister" structure expanding toward us, with the back side being the dense H II region itself.

4. DISCUSSION AND CONCLUSIONS

Massive stars are expected to produce wind-blown bubbles in the interstellar medium (Castor, Weaver, & McCray 1975; Weaver et al. 1977); however, main-sequence O stars are rarely seen surrounded by ring nebulae (Chu 1991). To search for wind-blown bubbles around main-sequence O stars, we have obtained high-resolution *HST* WFPC2 images and high-dispersion echelle spectra of two pristine H II regions, N11B and N180B, ionized by OB associations. The presence of O3 stars in these OB associations suggests that the H II regions are young and have not hosted any supernova explosion.

Analyzing the nebular morphologies and kinematics, we find that main-sequence O stars do blow bubbles in H II regions, and that the bubbles can be detected kinematically[11] but not morphologically. Most of these main-sequence bubbles have expansion velocities of 10–15 km s^{-1}, which is comparable to or slightly larger than the isothermal sound velocity of ionized gas at 10^4 K. The expanding bubbles generate only weak interstellar shocks as they expand into the ambient interstellar medium; therefore, no strong compression of the interstellar medium is expected in these bubbles. Lacking sharp filaments in Hα images, the slowly-expanding bubbles blown by main-sequence stars cannot be identified morphologically. Ironically, in N11B and N180B the morphological features that are conventionally identified as ring nebulae, such as a bright nebular arc around a star, are not expanding shells (e.g., MGSD 218 in N180B or PGMW 3120 in N11B).

Three types of wind-blown bubbles are seen in those young H II regions: (1) bubbles around concentrations of massive stars within which the projected separation between neighboring stars are typically ≤ 1 pc, (2) bubbles around individual O stars if the distance to neighboring stars is large enough to maintain the individuality of the bubble, and (3) a fossil bubble around an evolved red supergiant that is isolated. It is conceivable that the formation of wind-blown bubbles or superbubbles in an H II region depends crucially on the spatial distribution of the stars. Tight concentrations of massive stars are conducive to the formation of superbubbles even before any supernova explosion. Wide separations between massive stars are conducive to the formation of single-star, main-sequence bubbles, and a bubble may remain distinct even after the star has evolved into a red supergiant.

The observed expansion dynamics of the interstellar bubbles can be compared to those expected in bubble models of Castor, Weaver, & McCray (1975) and Weaver et al. (1977). With the observed radius (R in units of pc) and expansion velocity (V in units of km s^{-1}), we can compute the dynamical timescale (t_6 in units of 10^6 yr) using $t_6 = 0.6R/V$, and further determine the ratio of stellar wind luminosity (L_{36} in units of 10^{36} ergs s^{-1}) to ambient density (n_0 in units of H-atom cm^{-3}) using $L_{36}/n_0 = (R/27)^5 t_6^{-3}$. We adopt the rms densities we have determined for N11B and N180B, 15 H-atom cm^{-3} and 9.5 H-atom cm^{-3}, respectively. We have listed in Table 3 the observed diameter and expansion velocity of the expanding shells, together with the derived dynamical timescale and wind luminosity. We have also listed the early-type stars encompassed within each shell and the stellar wind luminosity expected from these stars.

We will focus on the two best-defined shells in our sample. First we consider the bubble blown by the O3–4 star MGSD 214 in N180B. With a radius of 11 pc and an expansion velocity of ∼20 km s^{-1}, the bubble around MGSD 214 has a dynamical timescale of 3.3×10^5 yr. Adopting N180B's rms density of ∼9.5 cm^{-3}, we find a wind luminosity of $\sim3\times10^{36}$ ergs s^{-1} for MGSD 214. This is a factor of 10 lower than that expected from an O3–4 star. Next we consider the bubble blown by PGMW 3204, 3209, and 3223 in N11B. The star PGMW 3209, while dominated by an O3III(f*) star, is in fact composed of at least 5 additional late O stars (Walborn et al. 1999). For a radius of 7 pc and an expansion velocity of 10 km s^{-1}, the dynamical timescale of this bubble is 4.2×10^5 yr. Using a rms density of 15 cm^{-3} for N11B, we expect a wind luminosity of $\sim2.5\times10^{35}$ ergs s^{-1} for PGMW 3209, two orders of magnitude lower than that expected from an O3III star. This discrepancy is even larger, if we consider the additional stars in PGMW 3209 and the neighboring stars PGMW 3204 and 3223.

The large discrepancy between stellar wind luminosities

[11] Note that the photo-evaporation of dense knots will produce line broadening (see simulations by Brandner et al. 2000), not the expanding shells we observed.

derived from observations and models of bubbles and those expected from the actual stellar content is very interesting. Similar discrepancy has been reported for circumstellar bubbles (e.g., NGC 6888; García-Segura & Mac Low 1995) and superbubbles (Oey 1996). Our results represent the first report for small interstellar bubbles. This discrepancy implies that either the observed stellar wind luminosities have been over-estimated or Weaver et al.'s model cannot describe the observed bubbles. If the observed stellar wind luminosity is correct, our observed bubbles will be too small and expand too slowly. To reduce the discrepancy, we need to increase the ambient density, but it is unlikely that we have under-estimated the rms density of the H II regions by factors of 10–100.

One further discrepancy underscores the deficiency of bubble models. The dynamical timescales of the bubbles in N11B, 0.1–0.5 Myr, are much shorter than the age of the OB association LH10, 2–3 Myr (Walborn & Parker 1992). A similar discrepancy is also observed in superbubbles (Oey 1996). These problems need to be seriously considered in the future.

The content and distribution of wind-blown bubbles in N11B are different from those in N180B: N11B has a larger number of wind-blown bubbles and faster-expanding bubbles. This difference is caused by the richness of massive stars in the encompassed OB associations. The OB association LH10 in N11B has 20 stars with stellar masses $M \geq 15$ $M_\odot$ (PGMW), while the OB association LH118 in N180B only has six (MGSD). Futhermore, LH10 has tighter concentrations of massive stars than LH118. Bubbles blown by concentrations of massive stars expand faster because of more powerful stellar winds. Therefore, N11B has more bubbles and the fastest expanding bubble is around its highest concentration of massive stars.

One property in common among the bubbles in N11B and N180B is the asymmetric structure – most of the bubbles are "blisters". A face-on blister can be diagnosed from the asymmetry in line profiles, which show a bright component near the H II region's systemic velocity and a faint component blue-shifted or red-shifted to higher velocities. A blister viewed from the side can be diagnosed by the displacement of the responsible star from the projected bubble center. As the stars in N11B and N180B are still young and must be located close to their birth places, their blister-like bubbles suggest that the stars are located near the surface of a dense cloud, where a density gradient is present; as opposed to embedded in the deep interior of a cloud, where the ambient density might be more uniform.

Finally, we note that numerous small dust clouds like Bok globules and elephant trunks are detected in N11B and N180B. If the ambient interstellar gas pressure is high enough, star formation might be triggered in these small dust clouds. At least one such cloud in N11B, the Y-shaped dust cloud near PGMW 3223, shows signs of on-going star formation at its tip. An infrared survey of N11B and N180B would reveal whether star formation has started in other small dust clouds.

We would like to thank Michael Dopita for prompt review and constructive suggestions. This research is supported by the STScI grant GO-06698.01-95A. Y.N. acknowledges the support from contract P4/05 "Pôle d'Attraction Interuniversitaire" (SSTC-Belgium) and from the PRODEX XMM-OM and Integral Projects. CD acknowledges the travel support from CTIO.

REFERENCES

Brandner, W., Grebel, E.K., Chu, Y.-H., Dottori, H., Brandl, B., Richling, S., Yorke, H.W., Points, S.D., & Zinnecker, H. 2000, AJ, 119, 292
Castor, J., Weaver, R., & McCray, R. 1975, ApJ, 200, L107
Chen, C.-H. R., Chu, Y.-H., Gruendl, R. A., & Points S. D. 2000, AJ, 119, 1317
Chu, Y.-H. 1983, PASP, 95, 873
Chu, Y.-H. 1991, in "Wolf-Rayet Stars and Interrelations with Other Massive Stars in Galaxies", IAU Symp. No. 143, ed. K. A. van der Hucht & B. Hidayat (Dordrecht: Kluwer), p. 349
de Jager, C., Nieuwenhuijzen, H., & van der Hucht, K. A. 1988, A&AS, 72, 259
García-Segura, G., & Mac Low, M.-M. 1995, ApJ, 455, 145
Garnett, D. R., Walsh, J. R., Chu, Y.-H., & Lasker, B. M. 1999, AJ, 117, 1285
Henize, K.G. 1956, ApJS, 2, 315
Hester, J. J., et al. 1996, AJ, 111, 2349
Holtzman, J. A., et al. 1995, PASP, 107, 156
Lucke, P. B., & Hodge, P. W. 1970, AJ, 75, 171
McKee, C. F., Van Buren, D., & Lazareff, B. 1984, ApJ, 278, L115
Massey, P., Garmany, C. D., Silkey, M., & DeGioia-Eastwood, K. 1989, AJ, 97, 107 (MGSD)
Oey, M. S. 1996, ApJ, 467, 666
Osterbrock, D. E., Fulbright, J. P., Martel, A. R., Keane, M. J., Trager, S. C., & Basri, G. 1996, PASP, 108, 277
Parker, J. W., Garmany, C. D., Massey, P., & Walborn, N. R. 1992, AJ, 103, 1205 (PGMW)
Peimbert, M., Rayo, J. F., & Torres-Peimbert, S. 1975, Rev. Mex. Astron. Astrof., 1, 289
Prinja, R. K., Barlow, M. J., & Howarth, I. D. 1990, ApJ, 361, 607
Rosado, M., Laval, A., Le Coarer, E., Georgelin, Y. P., Amram, P., Goldes, G., & Gach, J.L. 1996, A&A, 308, 588
Spyromilio, J. 1995, MNRAS, 277, L59
Walborn, N.R., & Parker, J.W. 1992, ApJ, 399, L87
Walborn, N.R., Drissen, L., Parker, J.W., Saha, A., MacKenty, J.W., & White, R.L. 1999, AJ, 118, 1684
Weaver, R., McCray, R., Castor, J., Shapiro, P., & Moore, R. 1977, ApJ, 218, 377

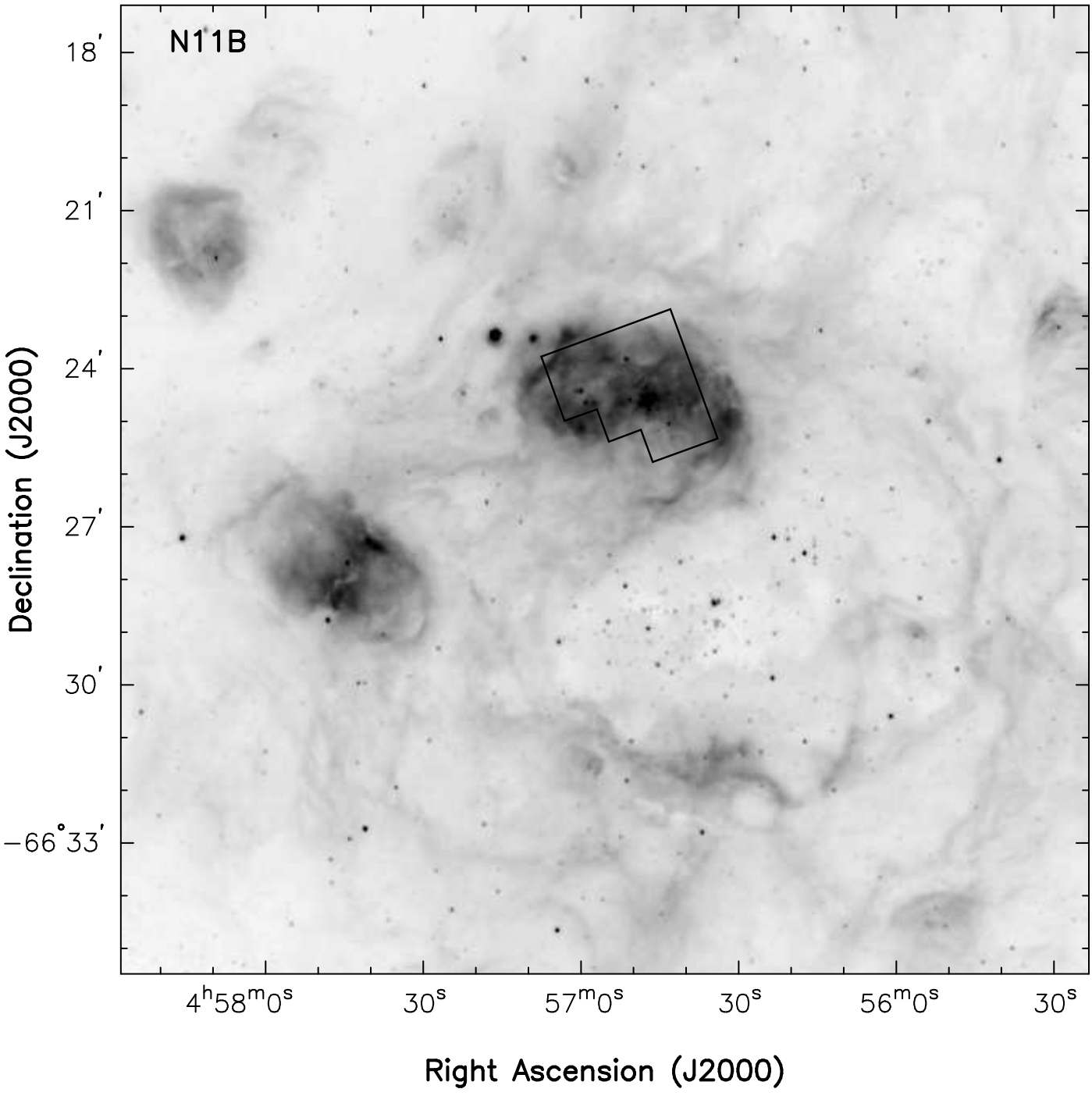

FIG. 1.— (a) Curtis Schmidt Hα CCD image of N11B with the WFPC2 field outlined.

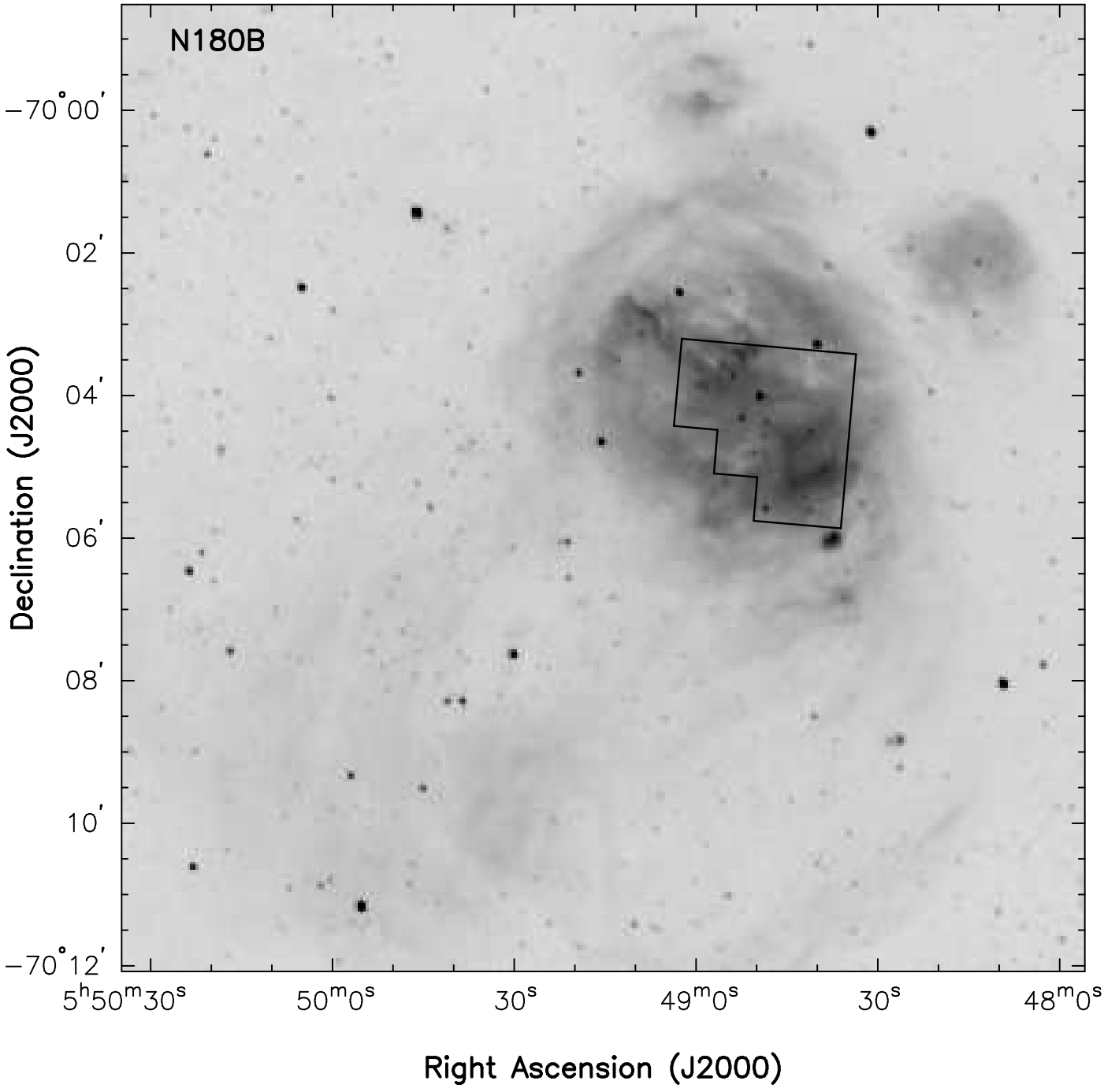

FIG. 1.— (b) Same as (a) for N180B.

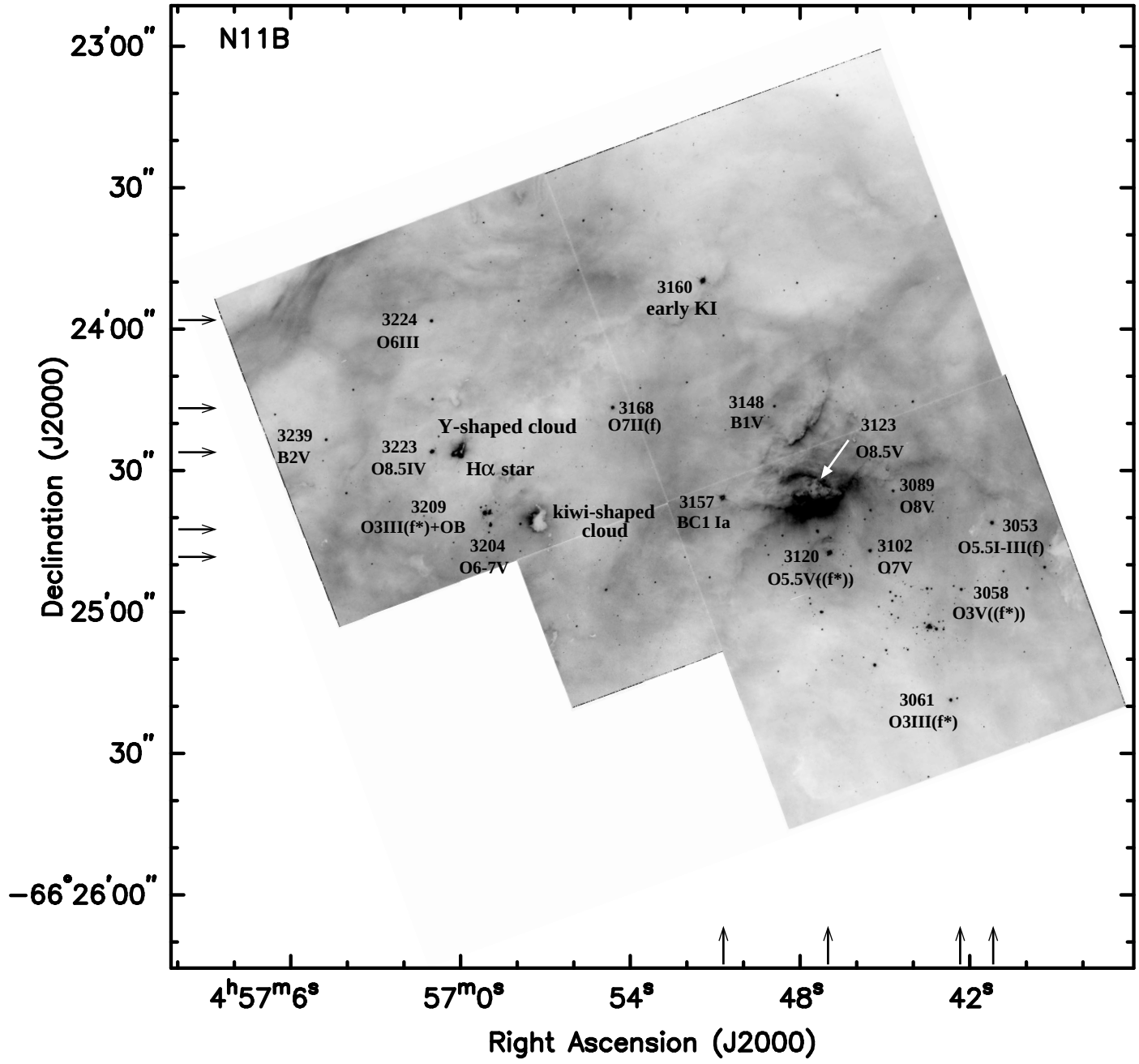

FIG. 1.— (c) *HST* WFPC2 Hα image of N11B. Stars cataloged by PGMW are marked with their catalog number and spectral classification. Slit positions of the echelle spectra are indicated by arrows.

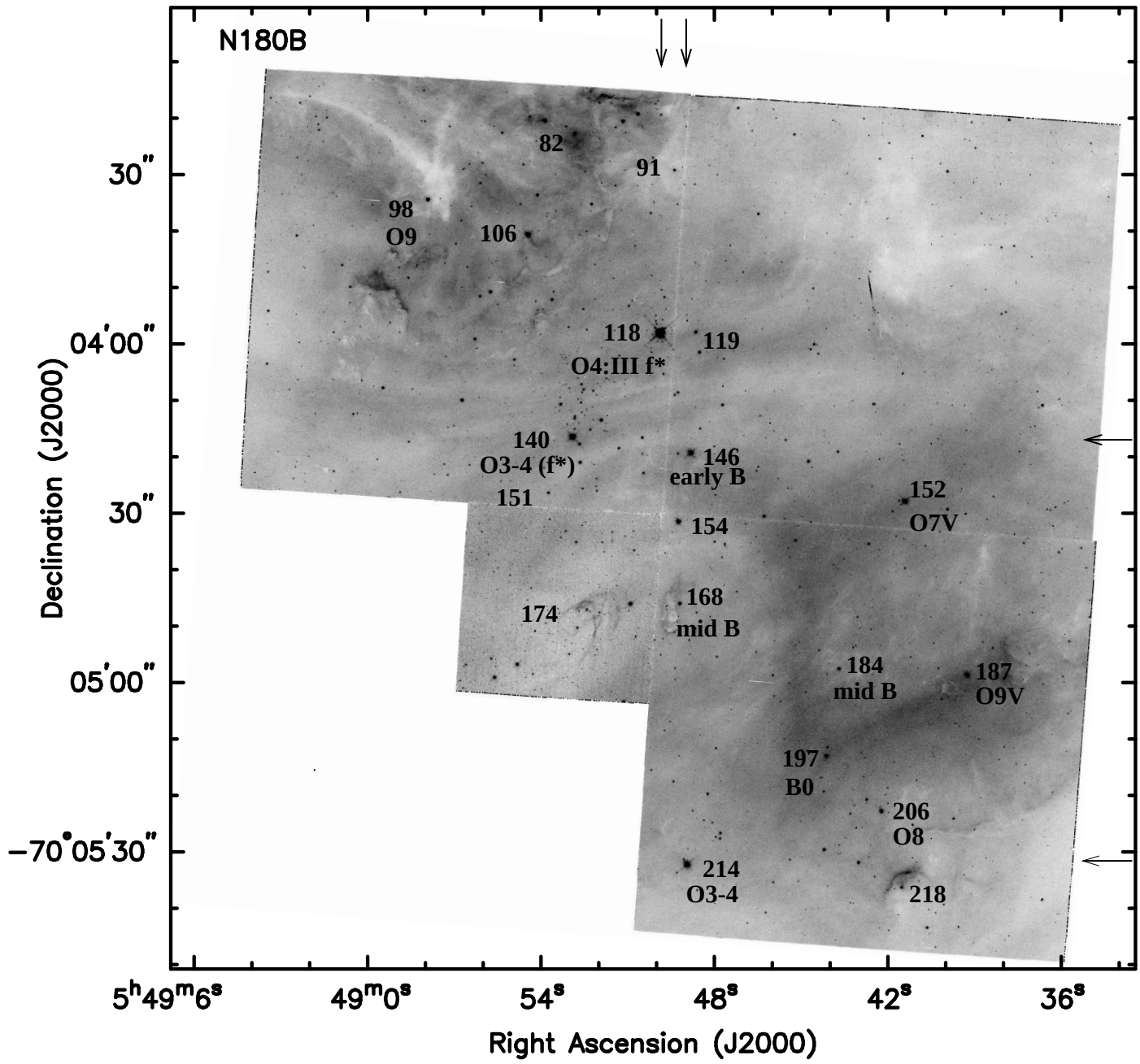

FIG. 1.— (d) Same as (c) for N180B. The star numbers and spectral types are taken from MGSD. Images presented in this article, except for Fig. 7, are negative images.

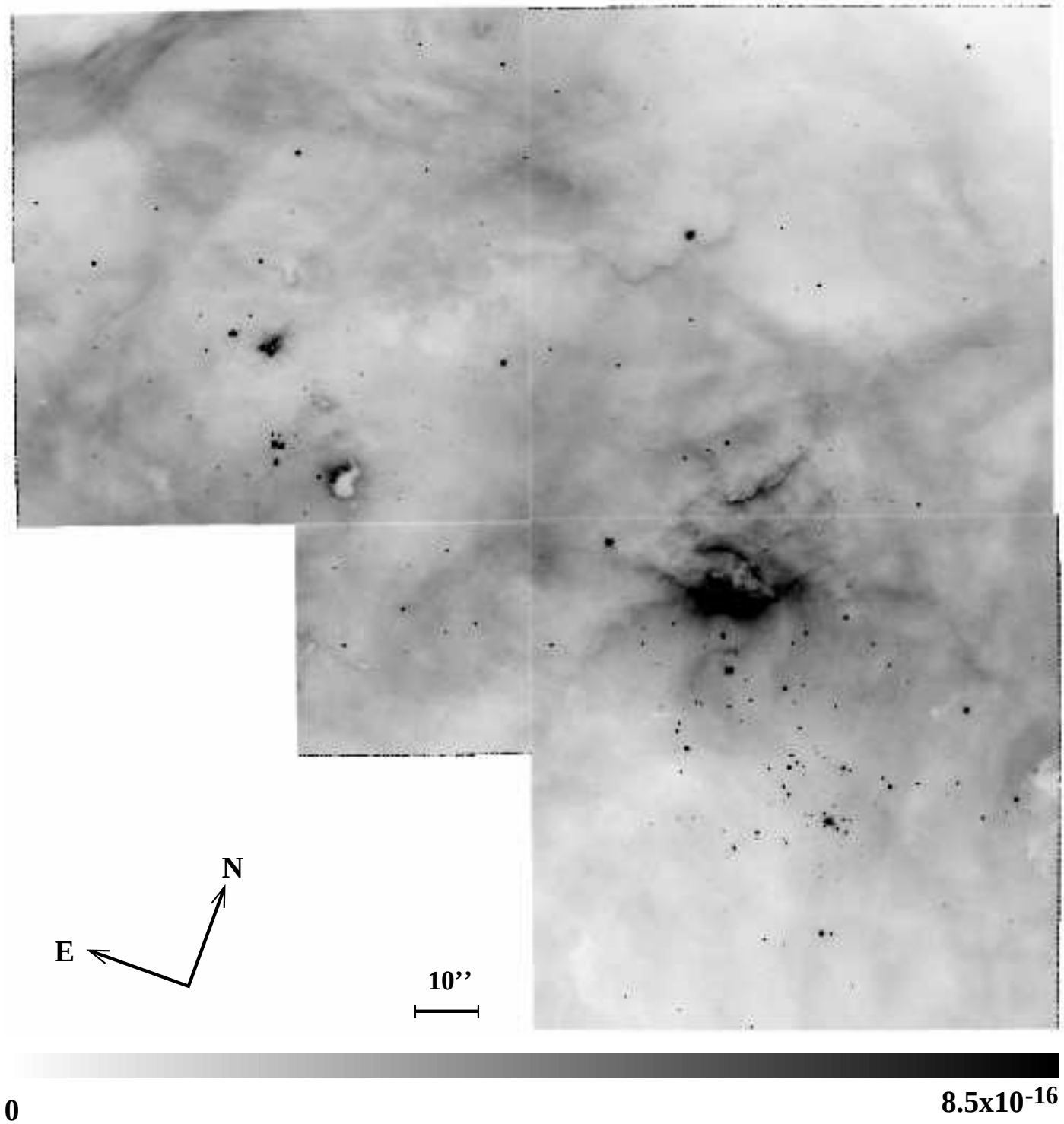

FIG. 2.— *HST* WFPC2 Hα image of N11B. The bar below the image shows the greyscale for surface brightness in units of erg $cm^{-2}s^{-1}$.

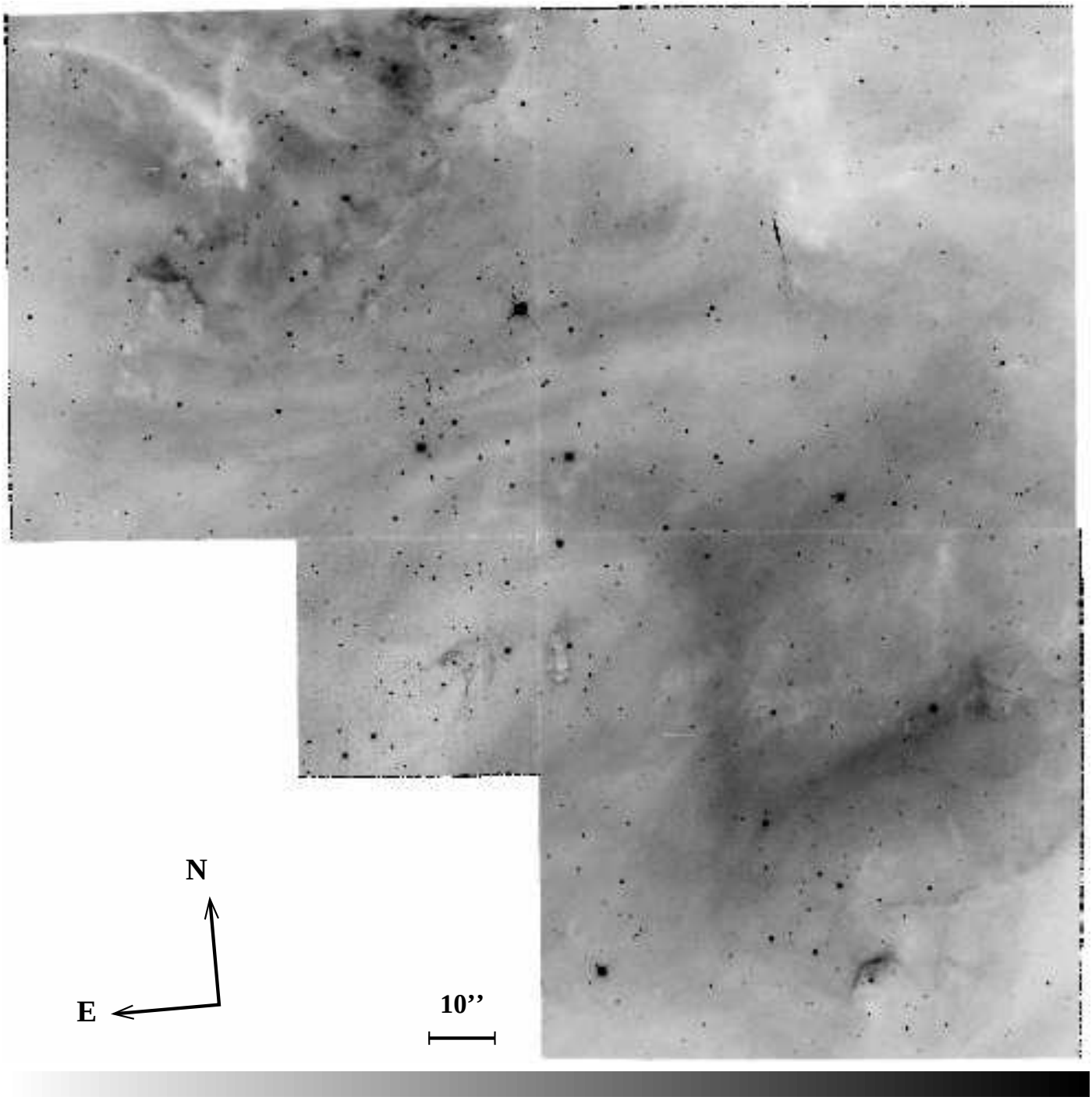

FIG. 3.— Same as Fig. 2, for N180B.

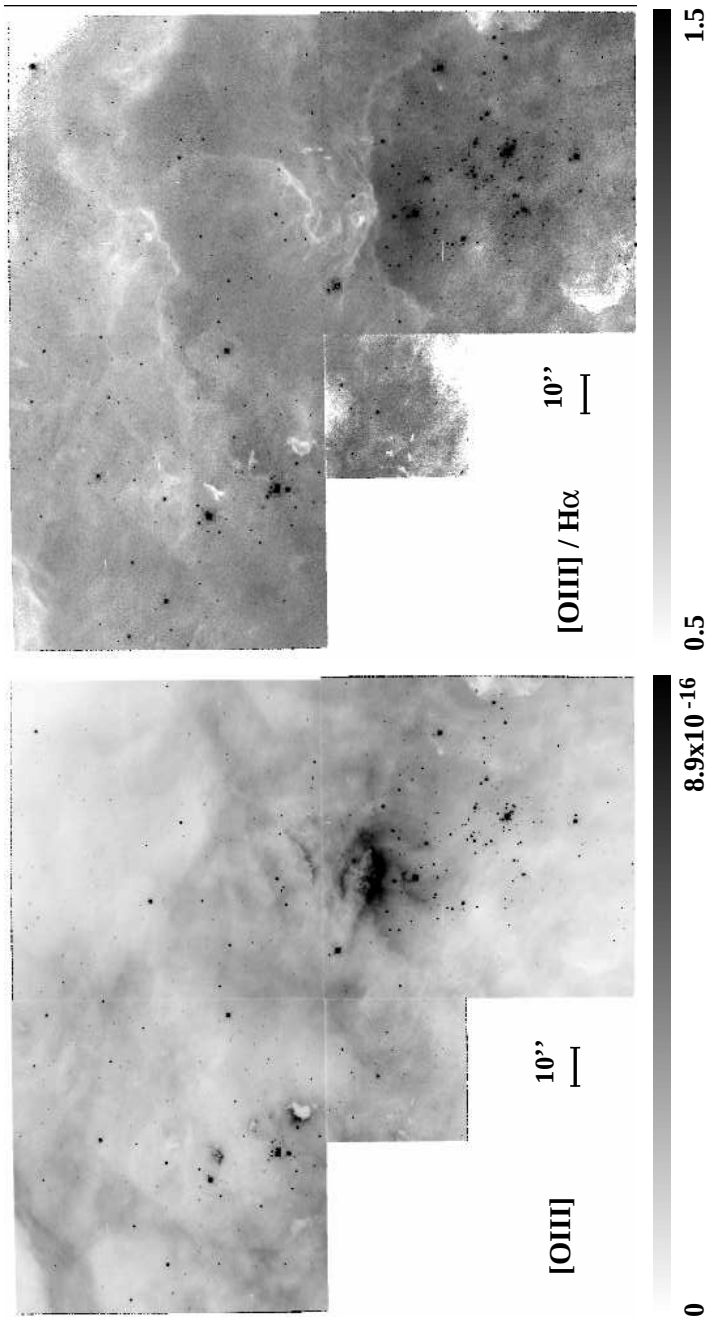

FIG. 4.— *HST* WFPC2 [O III] image (left) and [O III]/Hα ratio map (right) of N11B. The bars below the images show the greyscales for surface brightness (in units of erg cm^{-2}s^{-1}) and line ratio, respectively.

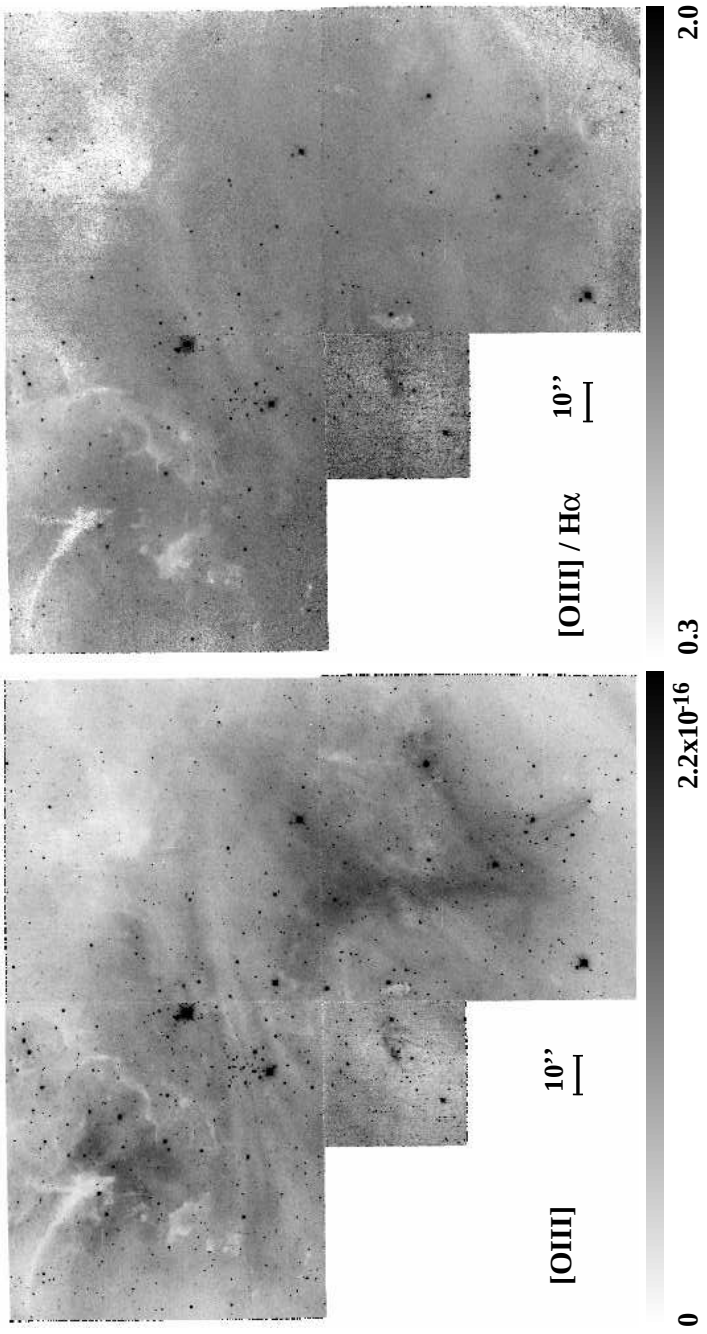

FIG. 5.— Same as Fig. 4, for N180B.

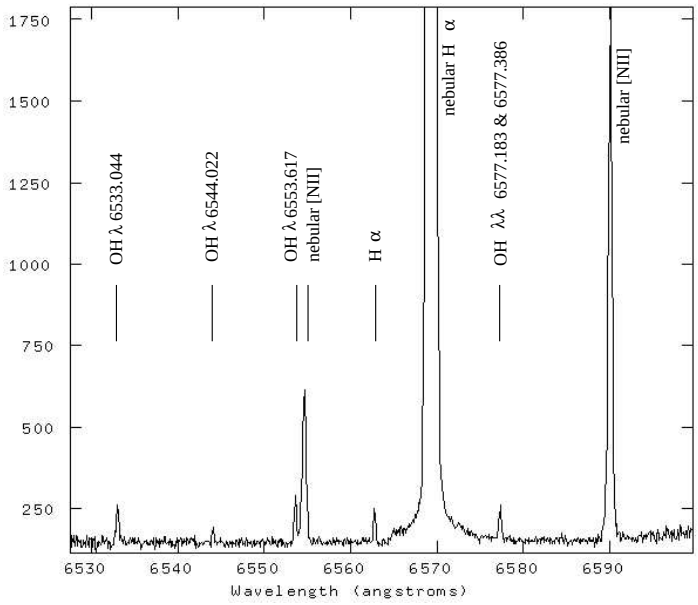

FIG. 6.— Identification of the telluric and nebular lines present in the echelle spectra of N11B and N180B. The telluric lines are narrow and unresolved. The intensity scale is arbitrary.

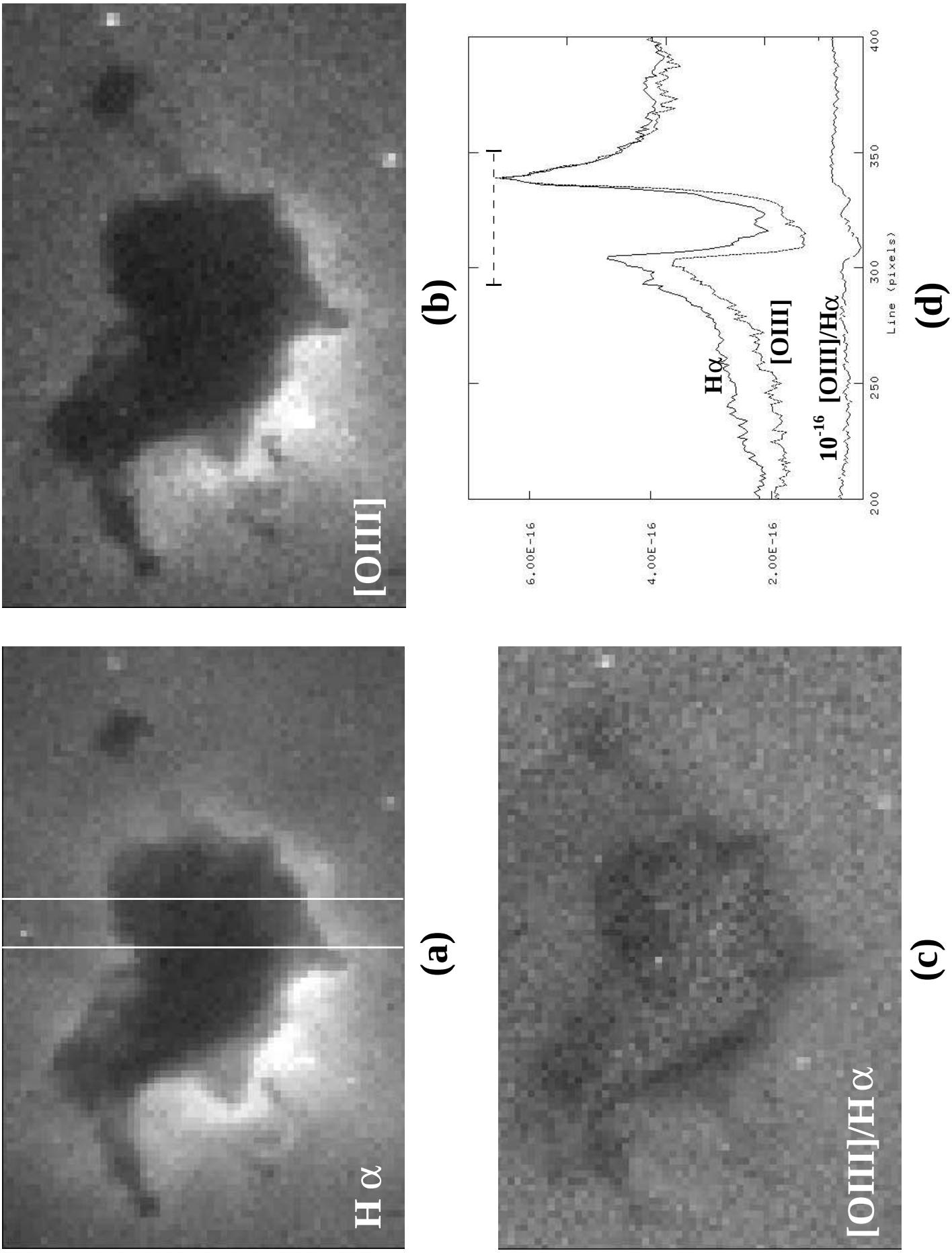

FIG. 7.— (a) *HST* WFPC2 Hα (b) [O III], and (c) [O III]/Hα ratio map of the kiwi-shaped dust cloud in N11B. The size of each image is $9'' \times 6''$. Note that these images are presented with emission in white, unlike the other figures. (d) Profiles of Hα and [O III] surface brightness, and the [O III]/Hα ratio (multiplied by 10^{-16}) along a cut bounded by the white lines on the Hα image in (a). The X-axis is in units of WFC pixel with a size of $0\farcs1$. The profiles plot extends further than the images shown in (a)-(c); the dashed line above the profiles marks the $6''$ extent.

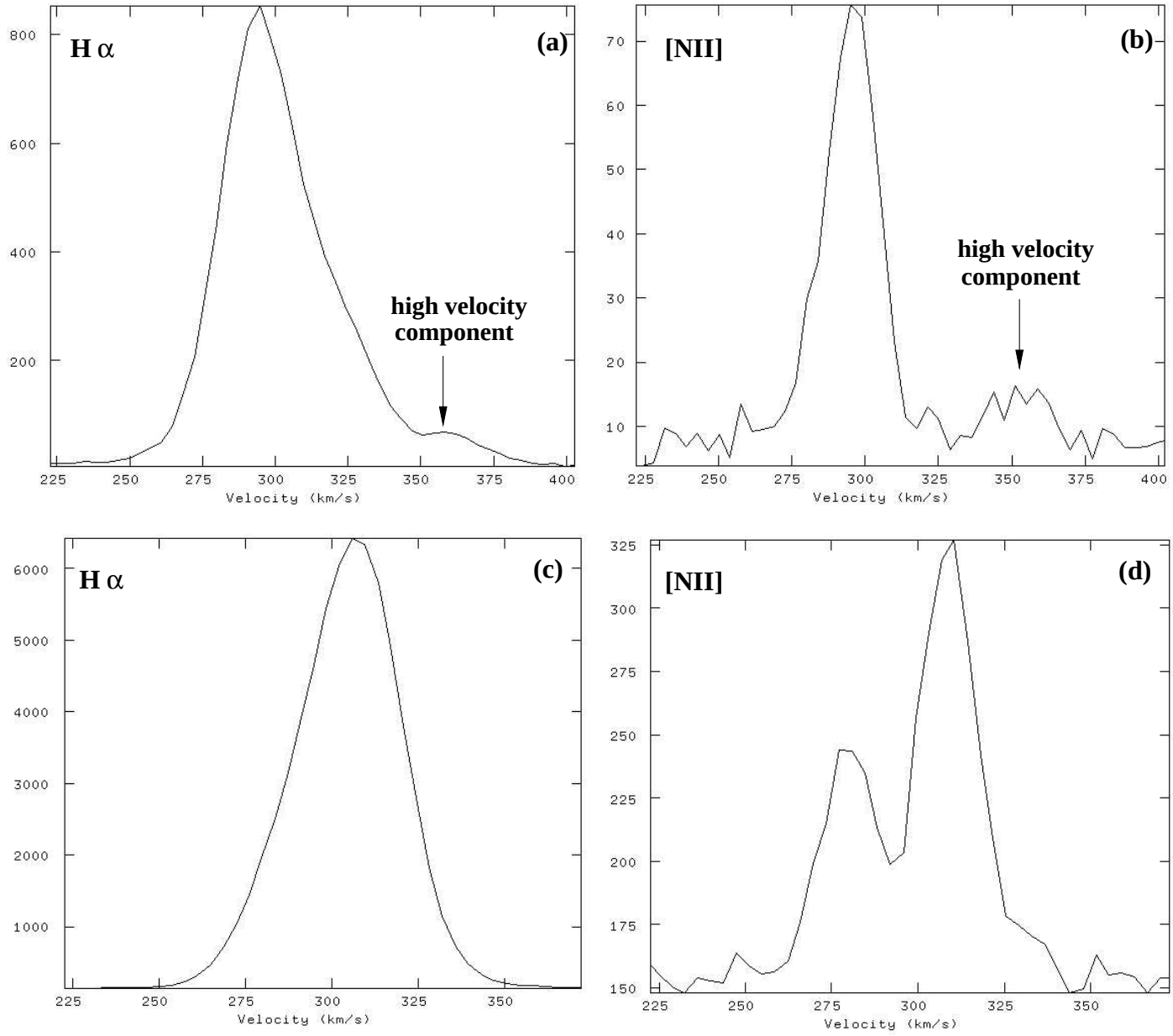

FIG. 8.— Examples of Hα and [N II] line profiles. (a) Hα and (b) [N II] profiles at 47.″5 south of PGMW 3053. (c) Hα and (d) [N II] profiles around PGMW 3120.

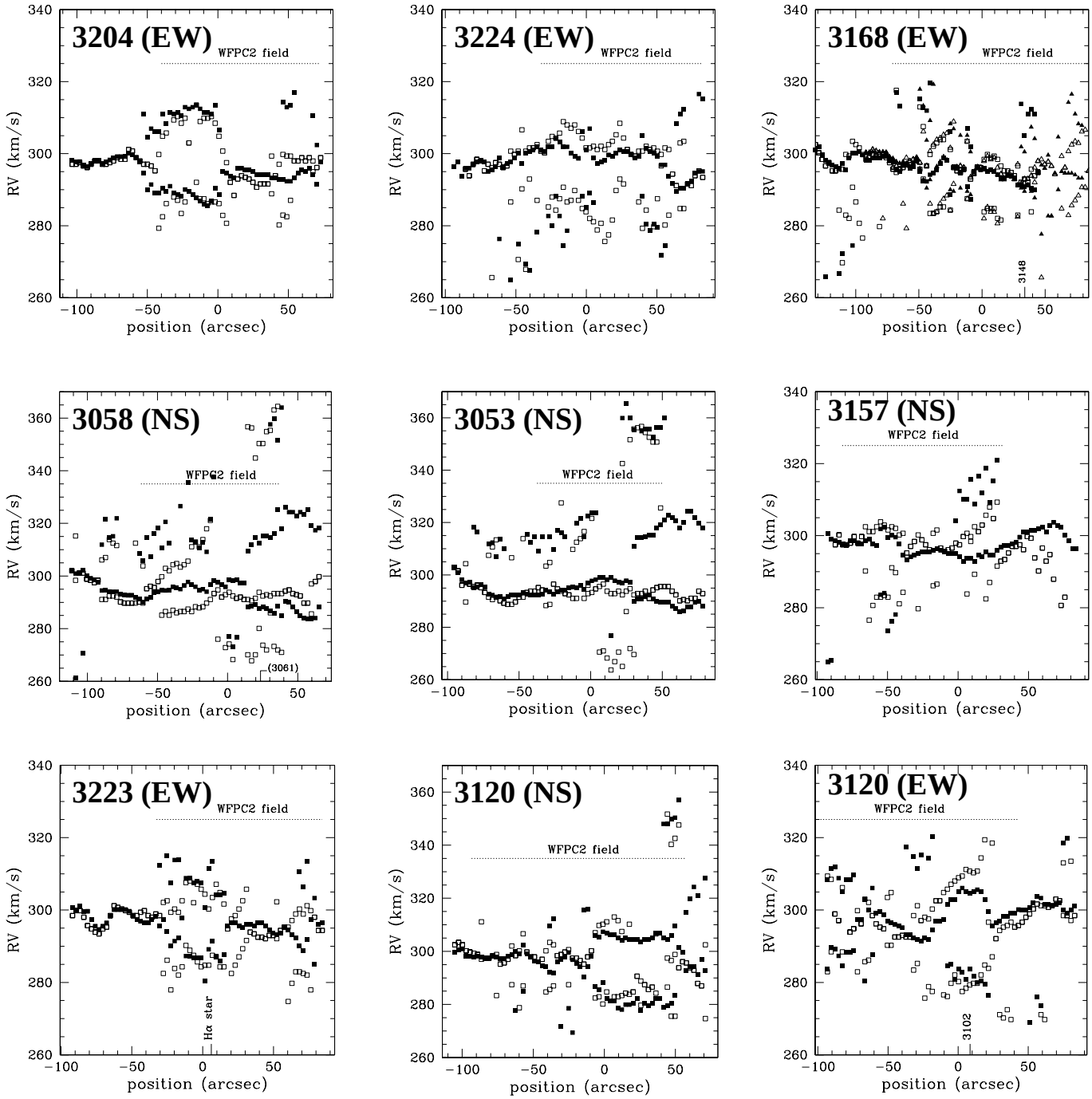

FIG. 9.— Radial velocity-position plots of the echelle slit positions in N11B for both Hα and [N II] lines. The radial velocities are heliocentric. The Hα velocity components are plotted in filled symbols, and the [N II] in open ones. The position axis is defined with the central star (labeled with its PGMW number at the upper left corner) at the origin ($0''$) and increasing towards south or west. When another star is present in the spectrum, its position is marked by a short vertical line labeled with its PGMW number. Stars close to the slit position are also marked but in parentheses. The dashed line in each plot indicates the range covered by the WFPC2 images. The two observations EW of PGMW 3168 were not centered at the same position; they were analyzed individually and plotted in different symbols, squares and triangles.

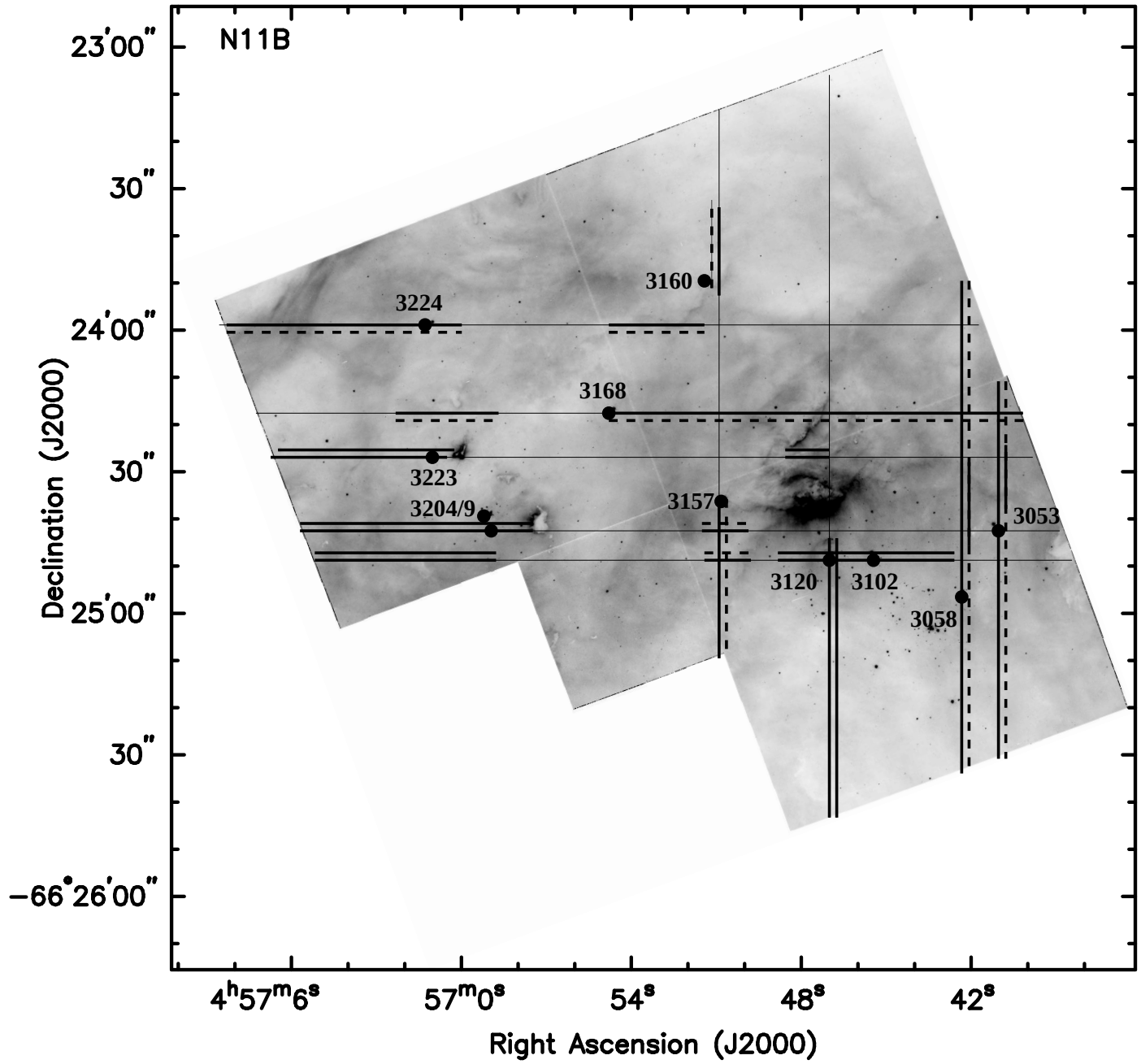

FIG. 10.— *HST* WFPC2 Hα image of N11B superimposed by spectral features: a thin line for a Gaussian profile, thick double lines for lines with clear splitting, and thick solid-dashed lines for asymmetric profiles indicating additional faint components. The relevant reference stars are also labeled. Note that the widths of the lines do not represent the slitwidth, which is 1.″65.

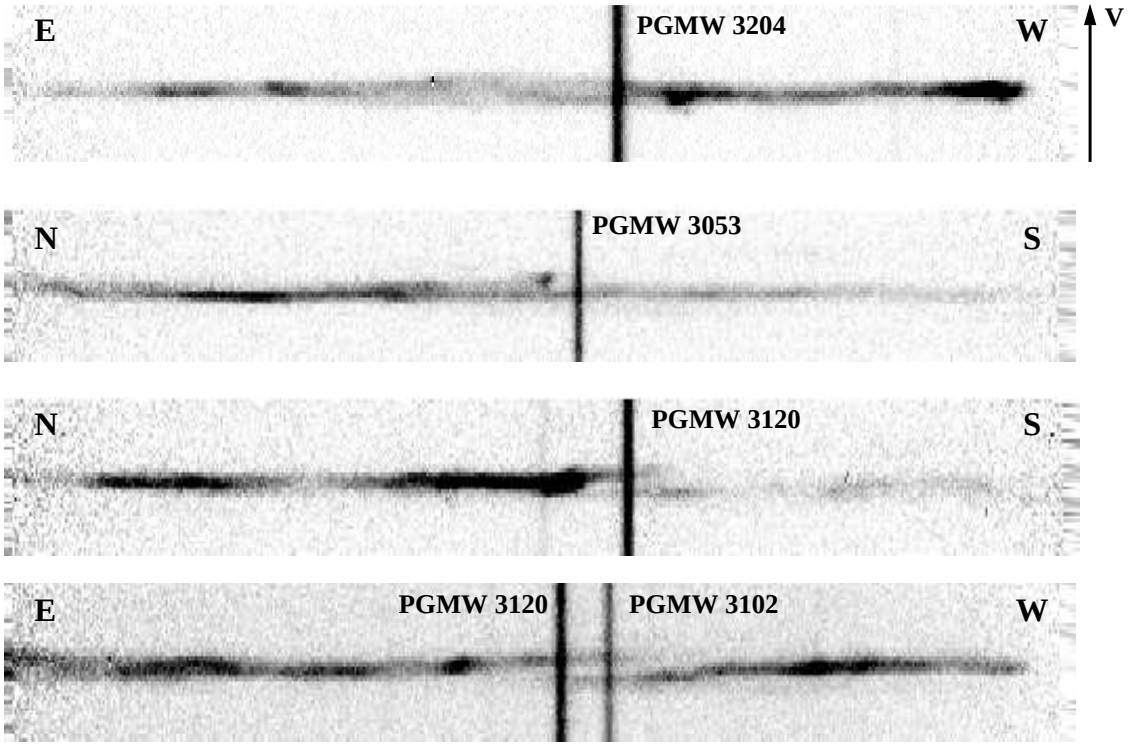

FIG. 11.— Four examples of echellograms of the [N II] line. The slit orientation and stars along the slit are marked. Each panel is 185″ along the horizontal direction and 200 $km s^{-1}$ along the vertical direction. The beginning of the splitting region seen to the north of PGMW 3053 is clearly marked by a bright knot in the spectrum. The line splitting around PGMW 3120 is clearly visible, while the "line splitting" region to the east of PGMW 3204 shows only a broad line.

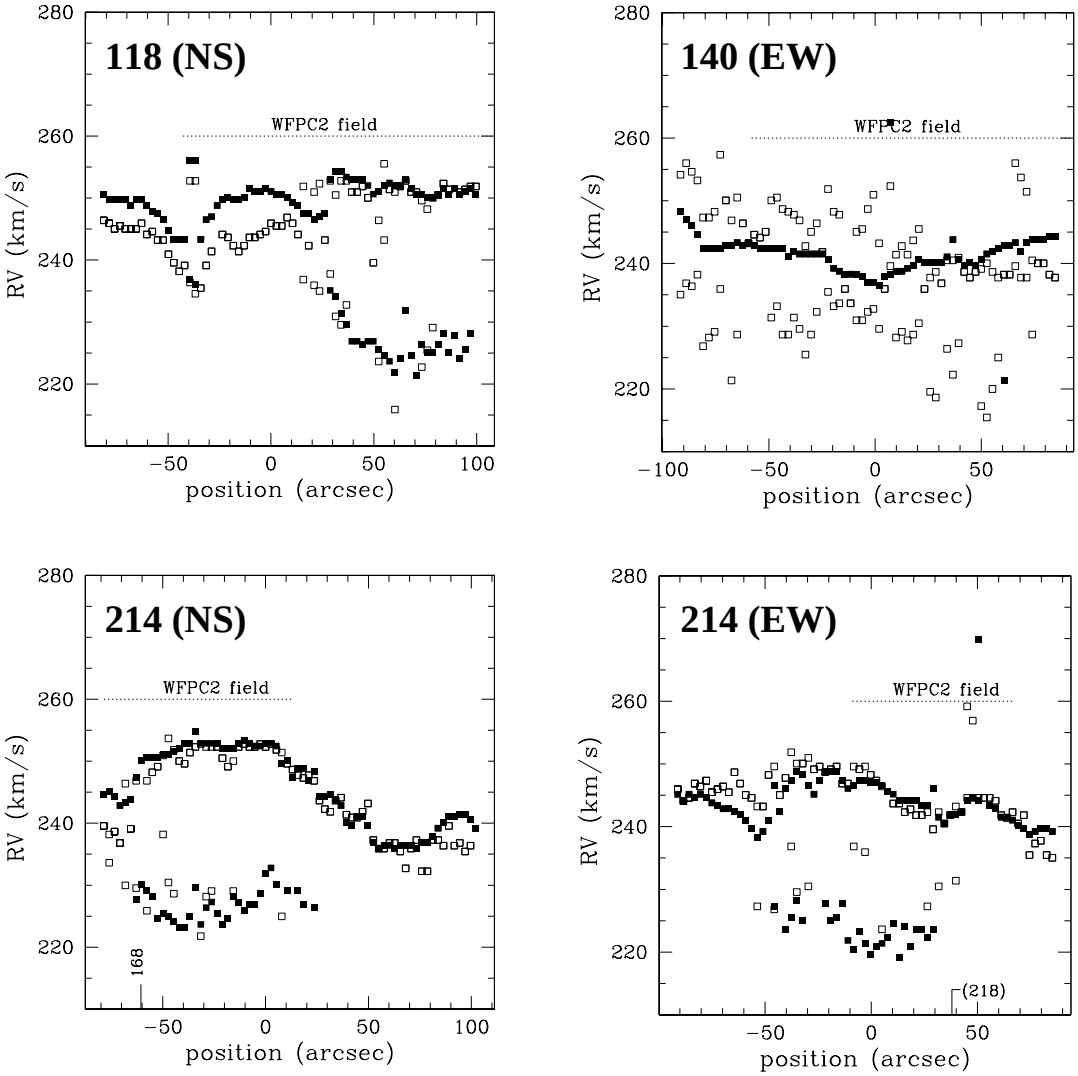

FIG. 12.— Same as Fig. 9, but for N180B. The star numbers are from MGSD.

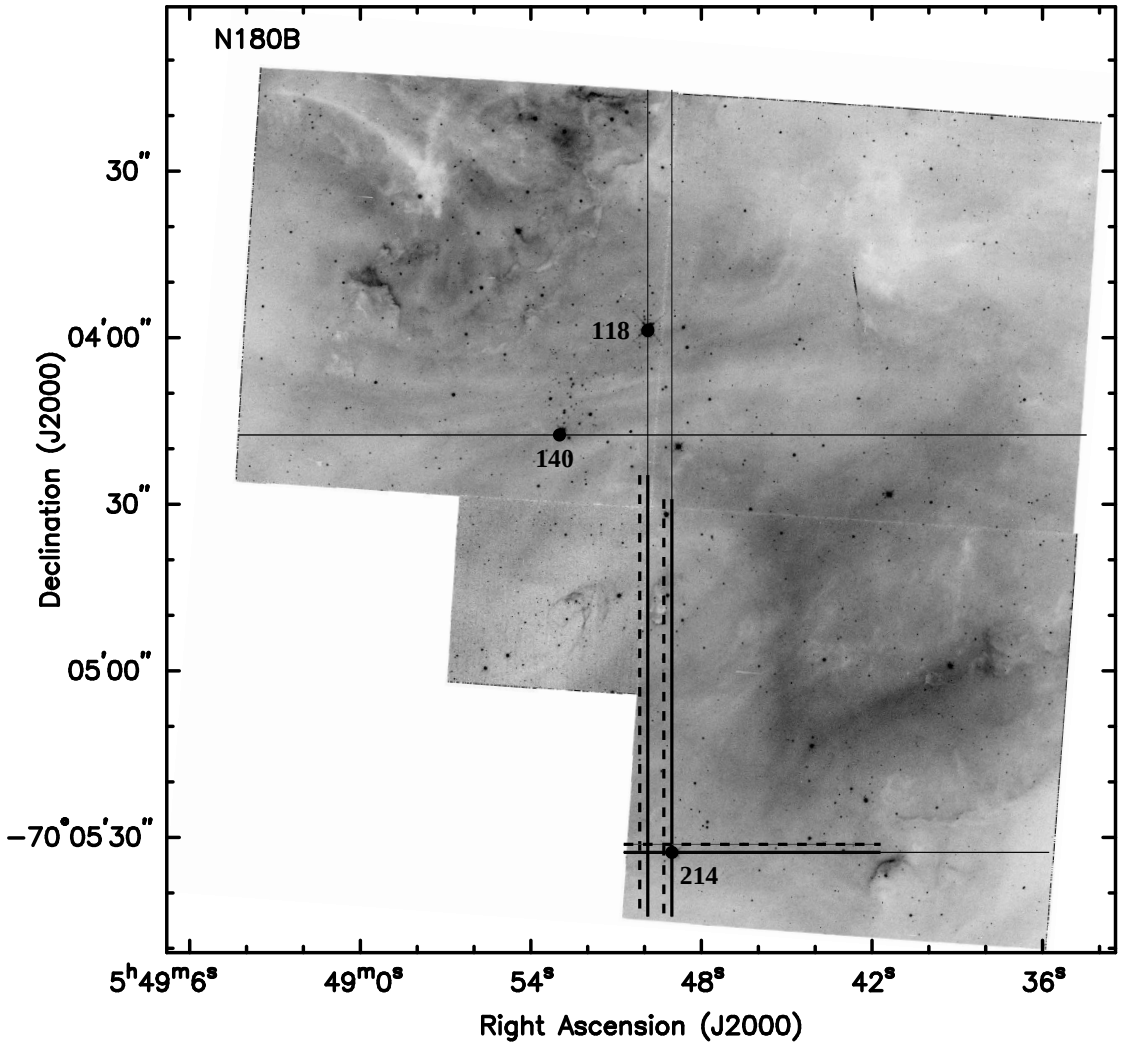

FIG. 13.— Same as Fig. 10, but for N180B. The star numbers are from MGSD.

Table 1
Journal of Echelle Observations.

Central Star	Slit Orient.	Exp. Time	Obs. Date
N11B			
PGMW 3204	EW	600s	2000 Jan 23
PGMW 3224	EW	600s	2000 Jan 23
PGMW 3168	EW	2×600s[a]	2000 Jan 23
PGMW 3058	NS	2×300s	2000 Jan 22
PGMW 3053	NS	2×300s	2000 Jan 22
PGMW 3157	NS	2×300s+10s	2000 Jan 22
PGMW 3223	EW	600s	2000 Jan 23
PGMW 3120	NS	2×300s	2000 Jan 22
PGMW 3120	EW	600s	2000 Jan 23
N180B			
MGSD 140	EW	600s	2000 Jan 23
MGSD 118	NS	600s	2000 Dec 10
MGSD 214	NS	600s	2000 Dec 10
MGSD 214	EW	600s	2000 Jan 23

[a] Two observations of PGMW 3168 were taken, but they were not centered at the same position.

Table 2
Densities of Selected Regions in N11B and N180B.

Region[a]	S(Hα) (10^{-3}erg cm^{-2}s^{-1}sr^{-1})	EM-EM$_{global}$ (10^4cm^{-6}pc)	Size ($''\times''$)	rms Density (cm^{-3})
N11B				
Near PGMW 3168(background)	0.955±0.016	(1.101±0.019)[b]	257×140	13-18
Arc S. of PGMW 3160	1.823±0.020	1.001± 0.030	17.8×1.5	50-160
Arc W. of PGMW 3148	3.280±0.028	2.683± 0.037	11.5×2.2	100-220
Arc N. of PGMW 3053	2.288±0.025	1.538± 0.035	7.8×2.8	90-150
Bright region of the kiwi cloud	5.096± 0.127	4.776±0.147	2.6×0.8	270-500
N180B				
Near MGSD 119 (background)	0.424±0.003	(0.489±0.004)[b]	225×225	9.5
S. of MGSD 214	0.297±0.002	(0.343±0.002)[c]	225×225	8
Arc N. of MGSD 218	0.696±0.007	0.314±0.009	5.4×1.3	50-100
V-shape zone between MGSD 187 and MGSD 197	0.764±0.002	0.392±0.005	37.0×7.0	20-50

[a] The different regions can be identified in Figs, 1c and 1d.
[b] This is the background reference, EM$_{global}$, and the size of this feature is the nebula's.
[c] This EM is not background subtracted.

TABLE 3
SUMMARY OF EXPANDING SHELLS PROPERTIES.

Ident.	Stellar content	L_w(stars) (10^{36} erg s^{-1})	Diam. (pc)	V_{exp} (km s^{-1})	t_6 (10^6 yr)	L_w(model) (10^{36} erg s^{-1})
N11B-1	all stars at the SW of N11B		$\geq$20[a]	20		
N11B-2	PGMW 3204 (O6-7V)	1.03	14	10	0.42	0.24
	PGMW 3209A (O3III(f*))[b]	15.8				
	PGMW 3209B (O9V)	0.14				
	PGMW 3209C (O7V)	0.59				
	PGMW 3209D (O9V)	0.14				
	PGMW 3209E (O9.5V)	0.03				
	PGMW 3209F (O9.5V)	0.03				
	PGMW 3223 (O8.5V)	0.08				
N11B-3	uncataloged star between PGMW 3223 and 3224		10	12	0.25	0.21
N11B-4	PGMW 3160 (early KI)		5	15	0.10[c]	0.10
N180B-1	MGSD 214 (O3-4)	13.4	22	20	0.33	2.97

[a] The insufficient spatial coverage of our echelle spectra to the south of N11B does not allow us to assign accurate boundaries to this expanding shell.

[b] The spectral types of components A–F are taken from Walborn et al. (1999)

[c] As the star is evolved, the bubble dynamics must have been modified, therefore these numbers may not be meaningful.